Stem Cell Reports
Report

ISSCR

OPEN ACCESS

Thyroid Progenitors Are Robustly Derived from Embryonic Stem Cells through Transient, Developmental Stage-Specific Overexpression of Nkx2-1

Keri Dame,[1,2] Steven Cincotta,[1,2] Alex H. Lang,[3] Reeti M. Sanghrajka,[1,2] Liye Zhang,[4] Jinyoung Choi,[1,5] Letty Kwok,[2] Talitha Wilson,[2] Maciej M. Kańduła,[6] Stefano Monti,[4] Anthony N. Hollenberg,[5] Pankaj Mehta,[3] Darrell N. Kotton,[1,2] and Laertis Ikonomou[1,2,*]

[1]Center for Regenerative Medicine, Boston Medical Center and Boston University, 670 Albany Street, 2nd Floor CReM, Boston, MA 02118, USA
[2]The Pulmonary Center, Department of Medicine, Boston University School of Medicine, Boston, MA 02118, USA
[3]Department of Physics, Boston University, Boston, MA 02215, USA
[4]Section of Computational Biomedicine, Boston University School of Medicine, Boston, MA 02118, USA
[5]Division of Endocrinology, Diabetes and Metabolism, Beth Israel Deaconess Medical Center, Harvard Medical School, Boston, MA 02215, USA
[6]Chair of Bioinformatics Research Group, Boku University, 1190 Vienna, Austria
*Correspondence: laertis@bu.edu
http://dx.doi.org/10.1016/j.stemcr.2016.12.024

SUMMARY

The clinical importance of anterior foregut endoderm (AFE) derivatives, such as thyrocytes, has led to intense research efforts for their derivation through directed differentiation of pluripotent stem cells (PSCs). Here, we identify transient overexpression of the transcription factor (TF) NKX2-1 as a powerful inductive signal for the robust derivation of thyrocyte-like cells from mouse PSC-derived AFE. This effect is highly developmental stage specific and dependent on FOXA2 expression levels and precise modulation of BMP and FGF signaling. The majority of the resulting cells express thyroid TFs (*Nkx2-1*, *Pax8*, *Foxe1*, *Hhex*) and thyroid hormone synthesis-related genes (*Tg*, *Tpo*, *Nis*, *Iyd*) at levels similar to adult mouse thyroid and give rise to functional follicle-like epithelial structures in Matrigel culture. Our findings demonstrate that NKX2-1 overexpression converts AFE to thyroid epithelium in a developmental time-sensitive manner and suggest a general methodology for manipulation of cell-fate decisions of developmental intermediates.

INTRODUCTION

Since tissue progenitors, giving rise to all mature cell types within a given tissue, are essential intermediates in embryonic development, their in vitro derivation has important implications for the fields of pluripotent stem cell (PSC) biology and regenerative medicine. Significant advances in anterior foregut endoderm (AFE) progenitor biology in recent years (Ikonomou and Kotton, 2015) have led to derivation of AFE lung and thyroid progenitors (TPs) and their clinically relevant progeny from PSCs (Green et al., 2011; Huang et al., 2014; Kurmann et al., 2015; Longmire et al., 2012; Mou et al., 2012). However, with one notable exception (Huang et al., 2014), efficiencies of progenitor derivation have been relatively low (<40%).

Overexpression of transcription factors (TFs) is a well-established approach to manipulate cellular identities as it results in reconfiguration or emergence of core TF networks, with derivation of induced PSCs from somatic cells being the most prominent example (Takahashi and Yamanaka, 2006). Inducible TF expression in PSCs has been used to potentiate the derivation of specific lineages and facilitate mechanistic understanding of cell specification (Bondue et al., 2008; Mazzoni et al., 2013; Petros et al., 2013; Seguin et al., 2008). For example, Costagliola and coworkers (Antonica et al., 2012) used forced overexpression of the thyroid TFs NKX2-1/PAX8 in mouse embryonic stem cells (mESCs) to produce thyrocyte-like cells with high efficiency (~60%) that formed in vitro follicular structures and rescued athyroid mice upon transplantation. However, studies that systematically investigate the mechanistic interplay between pulsed heterologous TF expression and developmental stages in directed differentiation of PSCs are lacking. To address this question, we used thyroid-directed differentiation (Kurmann et al., 2015) in combination with transient NKX2-1 overexpression as our model system.

Here, we report that transient expression of NKX2-1 functions as an inductive signal during thyroid-directed differentiation to convert AFE-stage cells to thyrocyte-like cells that self-organize to epithelial, follicle-like structures in 3D Matrigel culture. This thyroid conversion effect pertains only to a narrow developmental window of competence contingent on several parameters, including dual bone morphogenetic protein (BMP)/fibroblast growth factor (FGF) signaling and correct anterior patterning of definitive endoderm (DE). We employ emerging computational methods (linear algebra projections; Lang et al., 2014; Pusuluri et al., 2015) and genome-wide gene expression analysis by RNA-sequencing (RNA-seq) to demonstrate that the resulting cells are similar to mouse embryonic thyrocytes. Finally, we suggest using mathematical modeling that the induction effect is potentially governed by a time-dependent bistable switch.

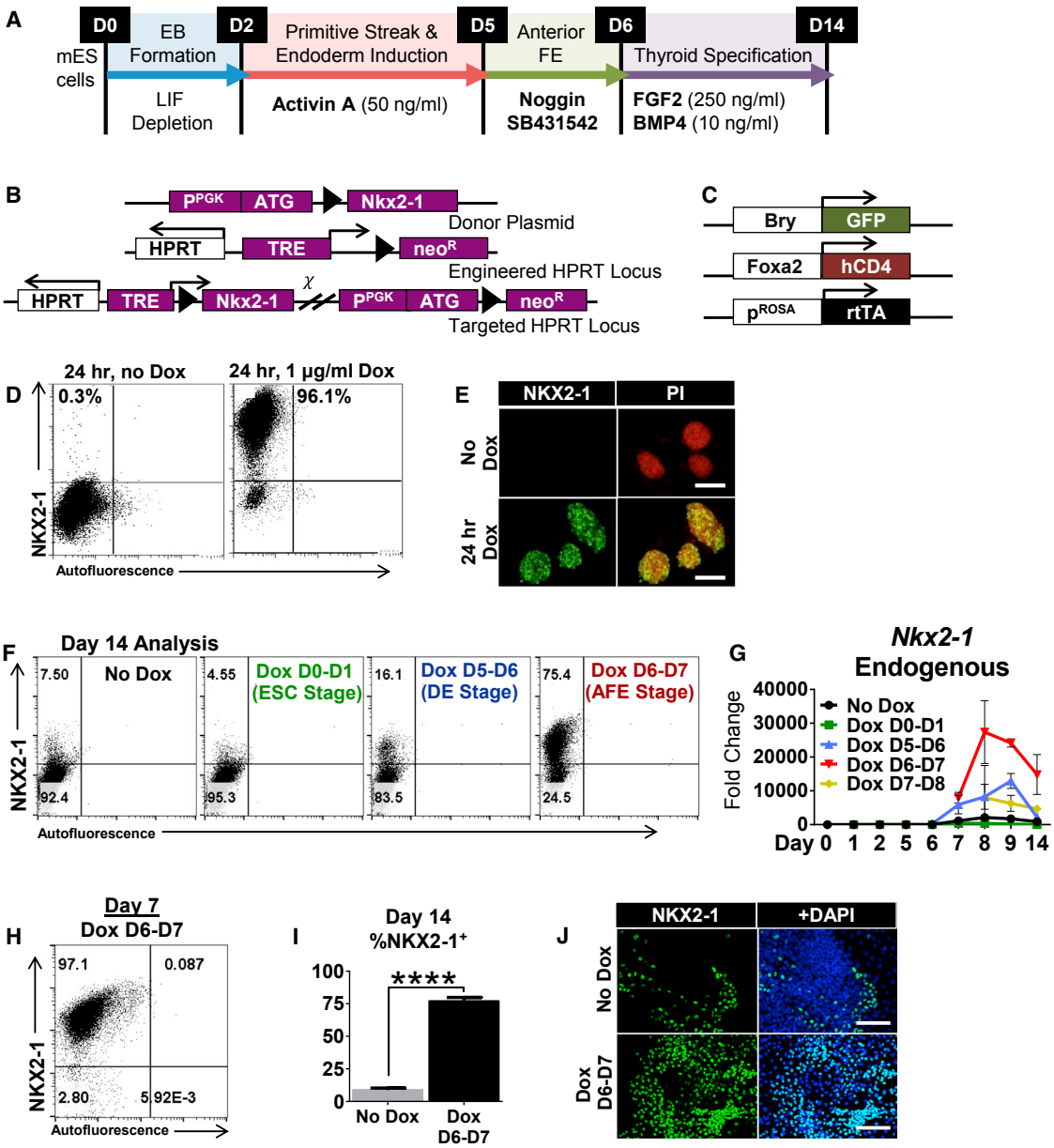

Figure 1. Stage-Specific Effect of *Nkx2-1* Overexpression on Derivation of NKX2-1$^+$ Progenitors

(A) Directed differentiation protocol for NKX2-1$^+$ TPs.

(B) Integration schematic of the Nkx2-1 transgene into the HPRT locus.

(C) Schematic of the knockin reporters (Brachyury^{GFP} and Foxa2^{hCD4}) and rtTA engineered into the iNkx2-1 line.

(D) Intracellular flow cytometry for NKX2-1 in undifferentiated cells with and without 24 hr of Dox treatment.

(E) Immunostaining of undifferentiated iNkx2-1 cells post-24-hr Dox; nuclear counterstain with propidium iodide (PI). Scale bars represent 100 µm.

(F) Intracellular NKX2-1 flow cytometry plots from D14 following 24-hr pulses of Dox added at indicated intermediate stages. Representative of three differentiations.

(G) Kinetics of endogenous *Nkx2-1* expression by RT-qPCR following 24-hr staged pulses of Dox. Fold changes relative to undifferentiated cells, error bars represent SD (n = 3 wells from same differentiation). Representative of three independent experiments.

(H) Representative flow cytometry plot of NKX2-1 expression directly post-24-hr Dox.

(legend continued on next page)

RESULTS

Efficient Temporal Control of Dox-Inducible Nkx2-1 Transgene Expression

We hypothesized that transient, temporally regulated *Nkx2-1* overexpression during directed differentiation of mESCs would lead to distinct differentiation outcomes due to differential competence of in vitro developmental stages. We created an mESC line (iNkx2-1) with a doxycycline (Dox)-inducible Nkx2-1 transgene (Figures 1B, 1C, S1A, and S1B) (Ting et al., 2005). This line was previously targeted with knockin reporters for *Foxa2* (Foxa2^{hCD4}) and *T* (Bry^{GFP}) (Gadue et al., 2006). The iNkx2-1 line displayed rapid on/off kinetics in response to Dox (Figures 1D, 1E, and S1C–S1E). Neither the transgene addition nor Dox affected pluripotency or standard directed differentiation (Figures S1F and S1G). This system allowed for efficient manipulation of NKX2-1 expression, resulting in robust induction of the Nkx2-1 transgene (>95% NKX2-1$^+$ cells by flow cytometry) following 24-hr exposure to Dox (1 μg/ml).

Stage-Specific Effect of Transient NKX2-1 Overexpression at the AFE Stage Results in Efficient Lineage Conversion

To test the temporal effects of *Nkx2-1* overexpression on thyroid derivation, we employed our iNkx2-1 cell line in combination with our thyroid differentiation protocol (Kurmann et al., 2015) (Figure 1A), which recapitulates key stages of thyroid development. In short, DE is induced by Activin A (Kubo et al., 2004), followed by further patterning to AFE (anteriorization) (Green et al., 2011; Longmire et al., 2012) using brief dual BMP/transforming growth factor β (TGF-β) inhibition through Noggin/SB431542 (NS) treatment, and specification to NKX2-1$^+$ TPs with BMP4 and FGF2 signaling. While this protocol is effective and reproducible, the yield is generally low (up to 25% NKX2-1$^+$ cells) with a fraction (~5%) coexpressing PAX8 (Kurmann et al., 2015), indicative of thyroid.

We first examined the effect of single 24-hr pulses of Dox-mediated transgene induction at biologically intermediate stages of differentiation. Parallel cultures received Dox at one of the following stages (D = day of differentiation): D0–D1 (exiting pluripotency); D5–D6 (DE stage); D6–D7 (AFE stage); or D7–D8 (early thyroid specification stage). In response to Dox, transgene activation resulted in >90%–95% NKX2-1$^+$ cells within 24 hr (Figure 1H and data not shown) at all time points and subsequently extinguished within 2 days of Dox withdrawal (Figure S1I). Not all intermediate stages of development demonstrated a lasting response to the NKX2-1 transgene overexpression, and a substantial increase of resulting NKX2-1$^+$ cells was highly restricted to a narrow window of induction at the AFE stage (Dox D6–D7) (Figures 1F and 1G). In addition, all other stages had low endogenous *Nkx2-1* expression immediately post-Dox (Figure 1G), showing a relatively weak response to the transgene overexpression (Oguchi and Kimura, 1998).

The effect of *Nkx2-1* overexpression at the AFE stage consistently resulted in a dramatic increase in the derivation of NKX2-1$^+$ cells (Figures 1I and 1J), indicating a singular competent stage where NKX2-1 acts as a lineage specification signal.

AFE-Stage NKX2-1 Overexpression Leads to Efficient Thyroid Derivation

Next we asked: does stage-specific, transient *Nkx2-1* overexpression potentiate the thyroid lineage or the derivation of non-thyroid NKX2-1$^+$ lineages? Early (*Pax8*, *Hhex*, *Foxe1*) and more mature (*Tg*, *Tpo*, *Nis*, *Tshr*, *Iyd*, *Dio1*) thyroid markers showed distinct activation kinetics along the differentiation course (Figure S1H) and were upregulated at D14 and D22 in the Dox D6–D7 induced cultures at levels comparable with in vivo purified NKX2-1^{GFP+} E13.5 thyrocytes (Longmire et al., 2012) and adult mouse thyroid tissue (Figures 2A and 2B). In addition, we observed extensive coexpression of NKX2-1 and PAX8 (Figures 2C, upper panel, 2D, and S2E) with the increasing presence of TG to D22/30 (Figures 2B–2D and S2E).

To test the functionality of our thyrocyte-like cells, we cultured cells in 3D Matrigel to induce organoid formation (Kurmann et al., 2015; Martin et al., 1993), which promoted expansion and maturation of the thyroid-like cells (Figure S2G) and organization into follicle-like structures (Figure S2F). These structures expressed NKX2-1, PAX8, E-cadherin, TG secreted into the follicle lumen, and importantly basolateral NIS, indicating maturation (Figure 2C). Following culture to D50 in maturation media (Figures 2E and S2H), organoids exposed to iodide produced T4 (Figures 2F and 2G), indicating full functional capability.

Although NKX2-1 is also critical for the development of the lung and forebrain (Kimura et al., 1996; Xu et al., 2008), we found minimal evidence of derived forebrain

(I) Averaged flow cytometry data (n = 12 independent experiments) comparing untreated (no Dox) and treated (Dox D6–D7) samples. Error bars represent SEM. ****p < 0.0001.

(J) Representative immunostaining of Dox-induced and uninduced cultures at D14. Scale bars represent 100 μm.

See also Figure S1.

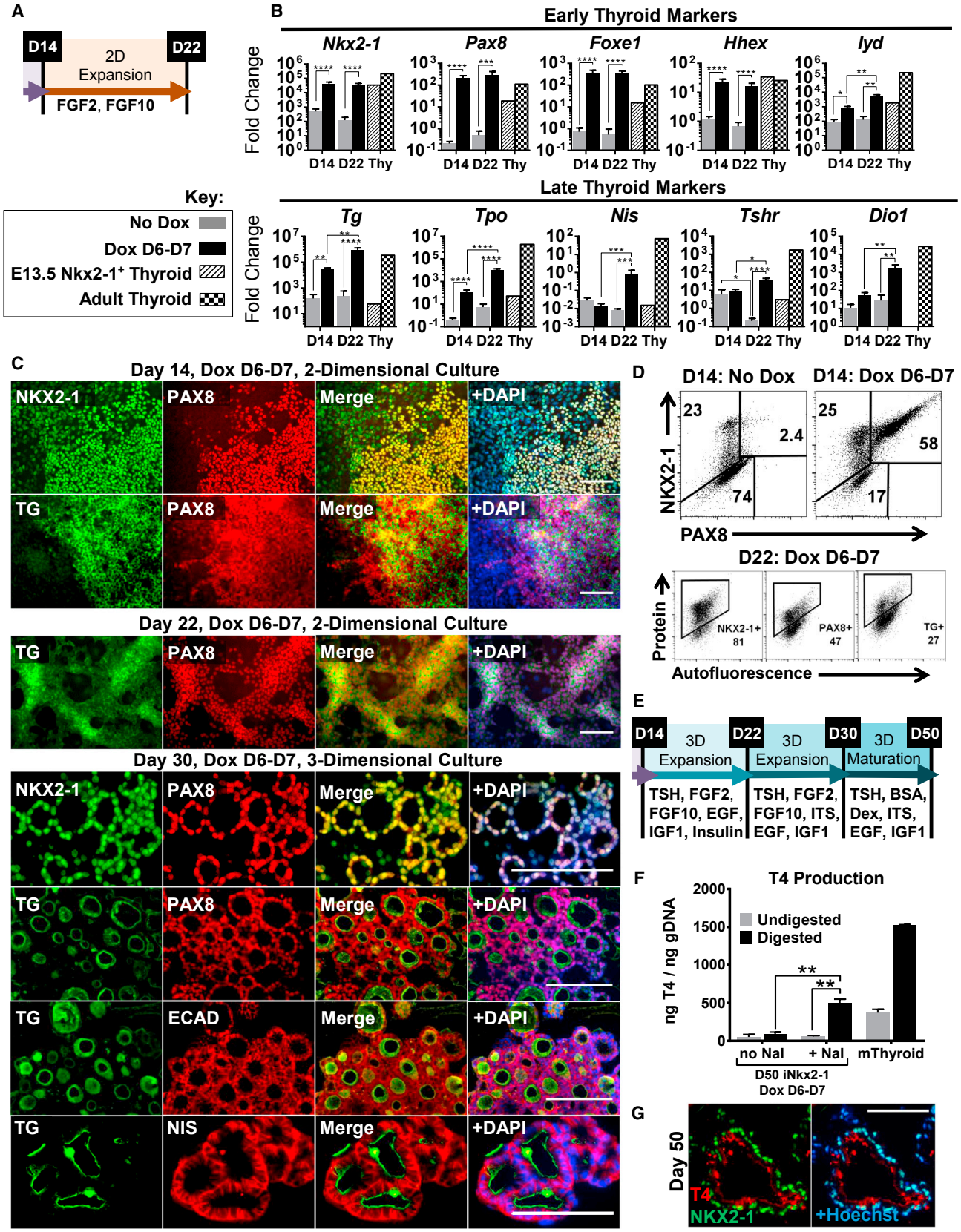

(legend on next page)

or neuronal lineages (Figures S2C and S2D), lung lineages (Figures S2A and S2B), or ectopic expression of liver or foregut markers (Figure S2D and data not shown).

These results show that overexpression of NKX2-1 can be used as an inductive signal to efficiently and robustly specify thyrocyte-like cells from AFE resulting in the derivation of in vitro cells exhibiting characteristics typical of murine thyrocytes.

NKX2-1-Induced Thyroid Specification Is Dependent on Efficient Derivation of AFE

Next, we sought to define the parameters of the robust AFE response to transient heterologous NKX2-1 expression. Omission of NS-mediated anteriorization at the DE stage, previously shown to be essential for lung/thyroid specification (Longmire et al., 2012), significantly reduced the percentage of NKX2-1^{+} cells, both with the standard and induced protocols (Figure 3A). More so, we found that abbreviation of this stage resulted in a time-proportional reduction in the D14 NKX2-1^{+} cell percentage (Figure 3B), demonstrating that the inductive effect of NKX2-1 overexpression is dependent on efficient AFE patterning.

Efficient Thyroid Conversion of FOXA2^{Neg} AFE Subpopulation

Next, we wanted to determine if the AFE contained subpopulations with variations in thyroid competency. We interrogated FOXA2 due to its dynamic expression kinetics during in vivo and in vitro foregut endoderm derivation (Fagman et al., 2011; Gadue et al., 2006) (Figures S3A–S3C).

We sorted cells at the AFE stage based on FOXA2^{hCD4} expression (Figure 3C) and replated with or without Dox (D6–D7). The population induced by FOXA2^{Neg}, relative to FOXA2^{High}, resulted in higher numbers of NKX2-1^{+} and NKX2-1^{+}PAX8^{+} cells (Figures 3D and 3E) and higher expression of thyroid markers (Figure 3F). In addition, no thyroid specification was observed from FOXA2^{low} mesoderm (Figures S3D and S3E) treated with Dox and cultured in thyroid specification media (Figure S3F). These results indicate the FOXA2^{Neg} population likely acquires this stage-specific thyroid competence through sequential progression from FOXA2^{+} DE to FOXA2^{Neg} AFE.

Combinatorial FGF2 and BMP4 Signaling Is Required for Thyroid Specification and Conversion

FGF2 and BMP4 have been identified as necessary and sufficient signals for thyroid specification in several species, including mouse (Kurmann et al., 2015). Withdrawal of either factor resulted in a severe loss of NKX2-1^{+} thyroid specification and thyroid marker expression, as well as reduced cell expansion in both uninduced and induced conditions (Figures 3G, S3G, and S3H). Last, Dox-treated pre-endoderm-stage cells cultured in various media including TGF-β/BMP inhibition followed by BMP4/FGF2 stimulation did not show thyroid competence (data not shown).

Taken collectively, these data demonstrate that only appropriately patterned AFE in conjunction with essential signaling pathways can specify at high efficiency to TPs in response to NKX2-1 overexpression.

Genome-wide Analysis of NKX2-1-Induced Thyroid Specification Reveals Putative Regulators of AFE Thyroid Competence

To gain further insights in the differential response to *Nkx2-1* overexpression, we performed RNA-seq on three populations (data available in GEO: GSE92572): Dox-induced D1 cells (minimal competence), Dox-induced D7 cells (AFE stage, maximum competence) and D14 cells, Dox D6–D7 (NKX2-1-induced TPs). Unsupervised hierarchical clustering and principal component analysis (PCA) demonstrated distinct transcriptional profiles by population (Figures 4A and 4B). Gene ontology analysis showed strong segregation of processes relating to differentiating cells (Figure S4A) and expression profiles confirmed the relevance of active BMP and FGF signaling pathways on D7 and D14 populations for thyroid specification (Figure S4B). To investigate the similarity of our populations to known cell types, we employed a linear algebra method using projection scores to measure cell similarity based on global gene expression (Lang et al., 2014; Pusuluri et al.,

Figure 2. Nkx2-1 Overexpression at AFE Stage Results in Efficient Thyroid Differentiation

(A) Experimental schematic of the extended culture conditions in (B), (C) (top three panels), and (D).

(B) RT-qPCR for thyroid marker expression. Fold changes calculated relative to undifferentiated cells, error bars represent SEM (n = 5 independent experiments, n = 1 control).

(C) Immunostaining of induced cultures at D14, D22 (gelatin substratum), and D30 (Matrigel embedded). Scale bars represent 100 μm.

(D) Intracellular flow cytometry for populations at D14 (top), separate differentiation single stains at D22 (bottom).

(E) Schematic of the maturation culture conditions for (F) and (G).

(F) T4 ELISA from D50 (Dox D6–D7) cells ± 10 μM NaI from D40 to D50 (n = 3 wells from the same differentiation). Mouse thyroid tissue for reference (n = 2 tissue samples).

(G) D50 immunostaining for +NaI cultures corresponding with (F). Scale bar represents 100 μm.

*p < 0.05, **p < 0.01, ***p < 0.001, ****p < 0.0001. See also Figure S2.

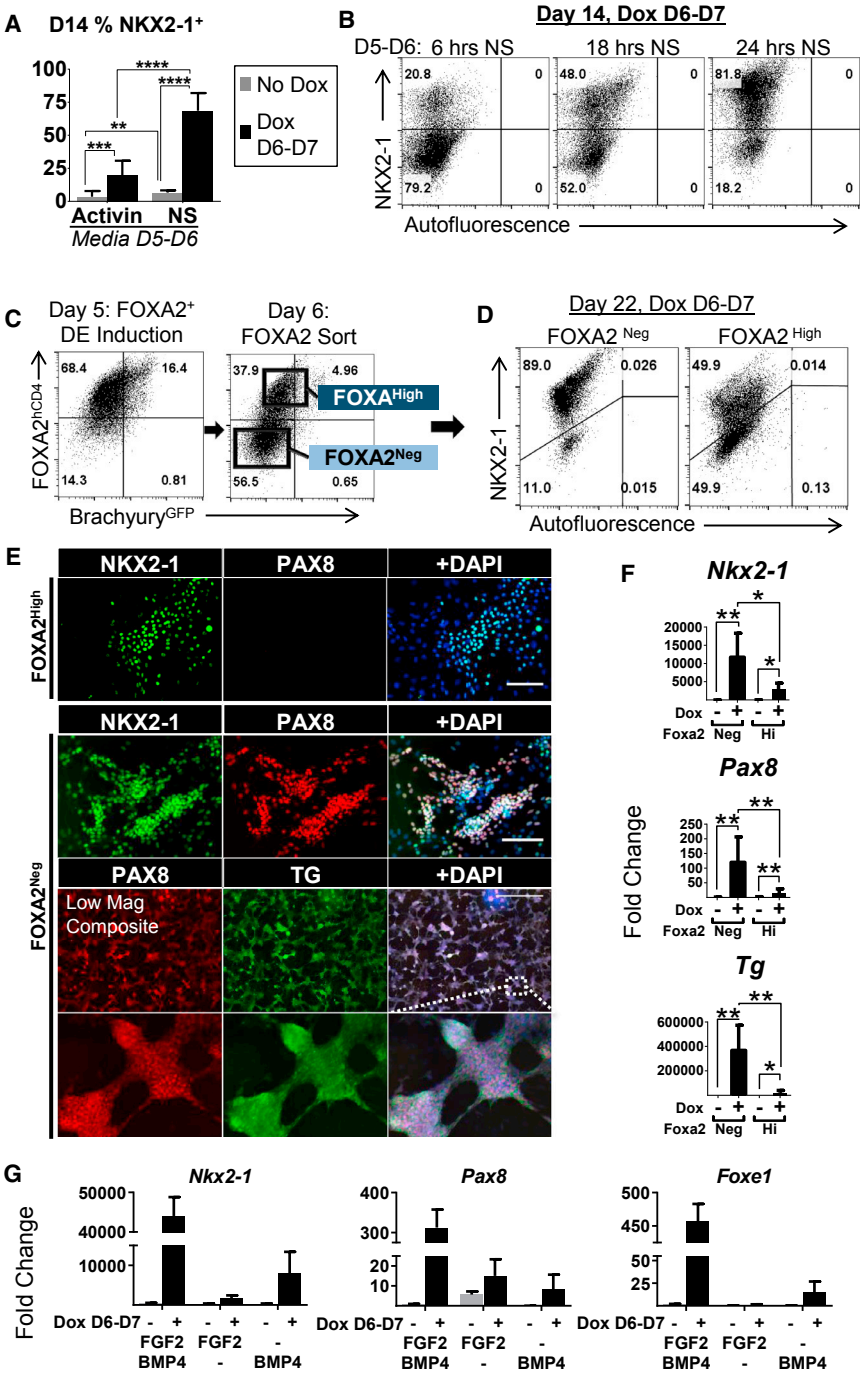

Figure 3. Efficient Thyroid Specification Is Dependent on Precise Modulation of BMP/FGF Signaling and Derivation of the Thyroid-Competent FOXA2^{Neg} AFE Population

(A) Intracellular D14 flow cytometry for NKX2-1 following D5–D6 NS or Activin treatment (n = 3 independent experiments).

(B) Intracellular D14 flow cytometry plots from varying duration of the anteriorization stage followed by 24 hr of Dox treatment.

(C) Flow cytometry sort schematic of D6 FOXA2^{+} AFE.

(D) Intracellular D22 flow cytometry from the sorted and induced populations shown in (C). Representative of three independent experiments.

(E) D22 immunostaining from FOXA2^{High} and FOXA2^{Neg} sorted populations. Top, scale bar represents 100 μm; bottom, scale bars represent 1,000 μm (composite image).

(F) D22 RT-qPCR data from the sorted populations shown in (C), with and without Dox D6–D7. Fold changes relative to undifferentiated cells, statistics from paired t tests, (n = 5 independent experiments).

(G) D14 RT-qPCR from induced and uninduced cells with specification factor variations. Fold changes relative to undifferentiated cells (n = 3 wells from same differentiation). Results are representative of three independent experiments.

*p < 0.05, **p < 0.01, ***p < 0.001, ****p < 0.0001. See also Figure S3.

2015). D14 cells projected strongly on purified E13.5 mouse Nkx2-1^{GFP+} thyrocytes, while D1 cells projected on mESCs, as expected (Figure 4C). Overall, these data suggest that transient NXK2-1 overexpression in the course of directed mESC thyroid differentiation does not fundamentally alter the identity of the derived TPs.

From two clusters of interest ("early" and "late") (Figures 4A and S4C), we identified potential transcriptional regulators and cell surface markers (CSMs) of thyroid fate (Tables S1 and S2). These lists contain genes with potentially novel roles in thyroid development, as well as genes previously implicated in foregut and early thyroid development both in vitro and in vivo (Fagman et al., 2011; Longmire et al., 2012; Millien et al., 2008). Of the early cluster CSMs, EPHB2 and SIRPA were identified to be highly expressed in DE (Figures 4D and 4E). Interestingly, *Ephb2* expression

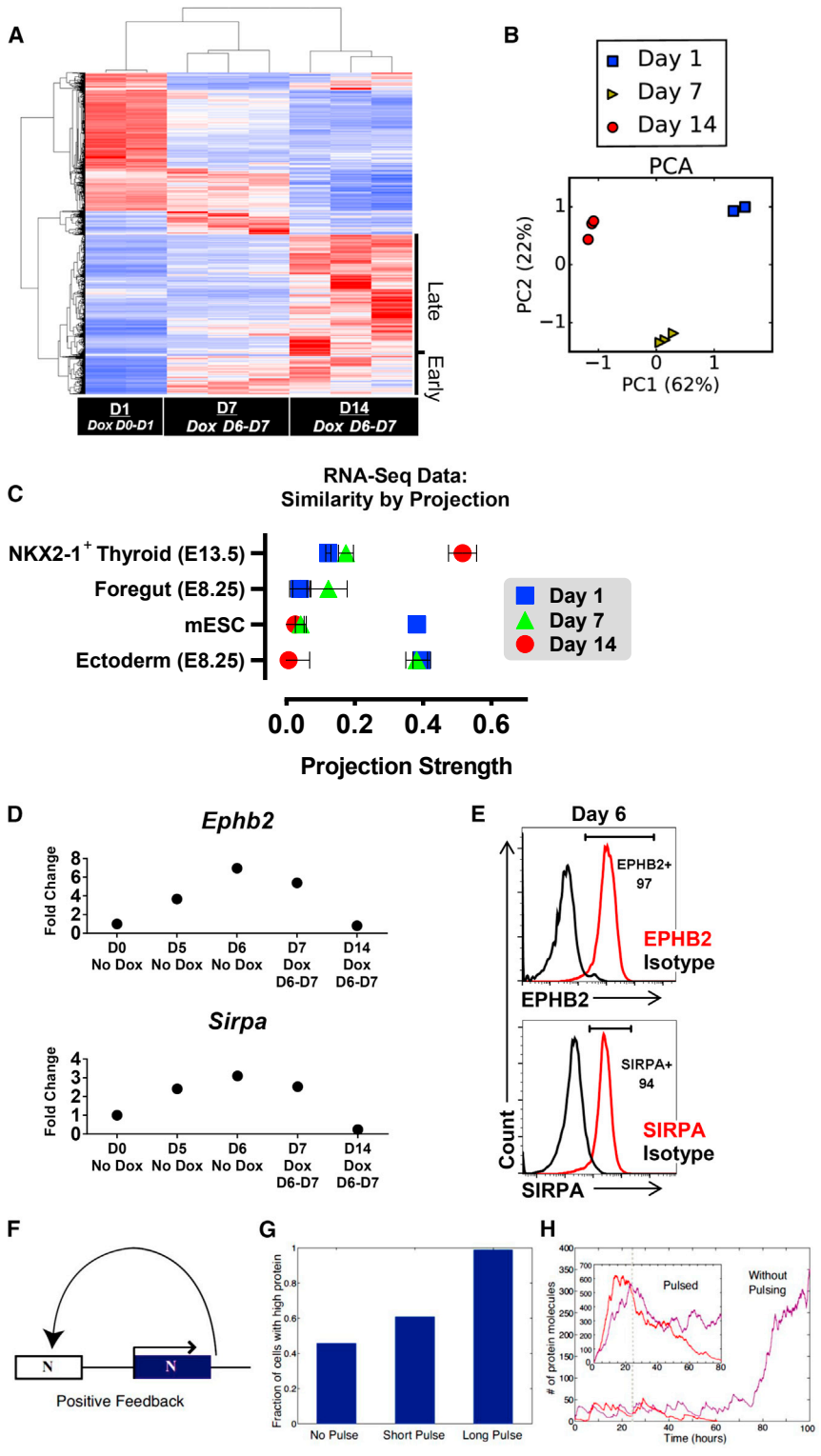

Figure 4. RNA-Sequencing Data Reveal Thyroid Signature

(A) RNA-seq heatmap of the top 9,088 differentially expressed genes with highest variance (false discovery rate <0.05) among samples, clustered by samples (columns) and genes (rows). Late and early clusters are indicated.

(B) PCA plot of RNA-seq populations.

(C) Projection graph representing the degree of similarity (x axis, exact match = 1) between RNA-seq samples (dots) and reference gene expression datasets (y axis).

(D) RT-qPCR validation data of cell surface markers identified in the early cluster.

(E) Flow cytometry data corresponding with (D).

(F) Bistable model: a protein that cooperatively binds its own promoter leads to a positive feedback-based, bistable switch.

(G) Percentage of high-protein-expressing cells in Monte-Carlo simulations of the bistable switch shown in (F) for three pulse lengths of protein expression. Results were calculated using 1,000 simulations in each condition.

(H) Stochastic trajectories of protein number as a function of time in the absence of pulsing (main figure) and in the presence of a long pulse (inset). Colored lines show stochastic trajectories that successfully activate the *Nkx2-1* feedback loop (purple lines) or fail to activate the feedback loop (red lines). The dashed line indicates the time the basal transcription rate was turned off in all simulations.

See also Figure S4.

in in vivo foregut endoderm was reported recently (Dravis and Henkemeyer, 2011). From the late cluster, reflective of a differentiated phenotype (Figure S4C), out of several CSMs correlating with the RNA-seq data, Col25a1 and Gabre were found to be enriched in both our induced and purified in vitro Nkx2-1$^{mCherry+}$ TPs (Figures S4D and S4E).

The Stage-Specific Effect of NKX2-1 Overexpression May Be Governed by a Bistable Switch

The central observation underlying our work is that activation of an Nkx2-1 transgene at different stages during thyroid-directed differentiation results in a wide percentage range of endogenous NKX2-1$^+$ TPs on D14 (Figure 1F). As NKX2-1 is known to bind its own promoter (Boggaram, 2009) and almost all cells are transgene NKX2-1$^+$ post-Dox induction (Figure 1H), the behavior of the system implies the existence of an AFE-stage-specific positive feedback loop at the *Nkx2-1* locus. This is further supported by the immediate activation of the endogenous *Nkx2-1* expression at the Dox D6–D7 condition (Figure 1G).

Based on these data, we modeled the D6–D7 cell response to the Dox pulse as a bistable switch (Ferrell, 2012), where the two states are "on" and "off" expression of endogenous *Nkx2-1* (Figures 4F–4H). Overall, this model could qualitatively reproduce our basic experimental observations, suggesting that a time-dependent bistable switch may underlie the effect of transgene overexpression on cell-fate decisions during directed differentiation of PSCs.

DISCUSSION

PSC-based systems hold great promise for the mass production of transplantable, clinically relevant cell types and for in vitro modeling of complex disease states. Currently, a major roadblock to achieving these goals is the poor or variable differentiation efficiency of many differentiation protocols. This study used developmental-stage-specific overexpression of a single TF, NKX2-1, to (1) investigate how cell competence changes in a dynamic, developmentally relevant system and (2) improve the efficiency of TP specification.

Our results demonstrate that the inductive effect of NKX2-1 is restricted to a singular stage of competence contingent on several synergistic parameters (FOXA2 levels, duration of anteriorization, and BMP4/FGF2 signaling), implying that AFE-staged cells possess a unique epigenetic status allowing for robust conversion to thyroid. Respiratory lineages were not derived as indicated by insignificant numbers of SPC$^+$ cells and the only presumed lung marker with high levels of expression (*Sftpb*) is expressed in both adult mouse (Figure S2A) and human thyroid (http://gtexportal.org/home/gene/SFTPB). We presume that the absence of Wnt agonists, an important signal for lung specification (Goss et al., 2009; Harris-Johnson et al., 2009; Huang et al., 2014), is the major reason for the paucity of respiratory lineages following NKX2-1 overexpression in our system.

Our study also achieved the practical goal of highly efficient thyroid differentiation. Our data indicate that the majority of the derived progenitors acquired a thyroid identity comparable with their in vivo counterparts, and importantly, their progeny gave rise to follicular-like structures in a 3D environment, expressed genes of thyroid hormone biosynthesis at levels comparable with adult thyroid, and produced high levels of T4 hormone. Overall, it appears that brief NKX2-1 exogenous expression during a well-defined window of maximum thyroid competence is sufficient to dramatically increase the yield and robustness of PSC thyroid specification and differentiation. Although a similar end-stage result has been previously reported through direct reprogramming of mESCs (Antonica et al., 2012), our approach delves into the mechanistic aspects of thyroid fate decisions and competence at a developmentally relevant stage. Further work is needed to define whether the thyrocyte-like cells produced downstream in our system are functionally equivalent to the reprogrammed cells and to the progeny of purified bona fide TPs (Kurmann et al., 2015).

This system can also be useful as a discovery tool in the absence of lineage-specific reporters. Analysis of the RNA-seq has identified both CSMs as well as potential regulators of thyroid fate in AFE and early TPs. Some of the TFs identified (*Irx5*, *Hoxb8*, *Isl1*) have been involved in mouse foregut and thyroid development (Millien et al., 2008; Westerlund et al., 2008), while others, such as *PROX1*, have been implicated in human thyroid disease (Ishii et al., 2016). Future PSC-based and in vivo studies will unravel the thyroid-related function of select TFs during thyroid specification and development.

Our theoretical model proposes a bistable positive feedback loop as the underlying mechanism to describe the endogenous *Nkx2-1* locus activation at the AFE stage leading to subsequent stabilization of the core TF network, establishing thyroid identity. Future work will focus on experimental validation of the model and investigate the possibility that bistable switches controlling bifurcation dynamics in cell-fate decisions (Loh et al., 2014) can lead to the development of highly efficient and robust protocols of general applicability.

EXPERIMENTAL PROCEDURES

All mouse work was approved by the Institutional Animal Care and Use Committee of Boston University School of Medicine.

Generation and Characterization of Inducible Line

The Ainv15 mESC line (Kyba et al., 2002) was a kind gift from Dr. Paul Gadue. As previously described (Ting et al., 2005), this line was engineered with a constitutively expressed rtTA from the Rosa26 locus and a promoter with tetO sites upstream of a *loxP* site at the HPRT locus. The Nkx2-1 transgene was inserted via co-electroporation of the plox-Nkx2-1 and pSalk-Cre plasmids.

Colonies with restored neomycin resistance were screened for efficient Dox-mediated Nkx2-1 induction.

mESC-Directed Differentiation

Directed differentiation was performed in serum-free media as previously described (Kurmann et al., 2015; Longmire et al., 2012) (see Supplemental Experimental Procedures for detailed description).

Statistical Analysis

Error bars in graphs represent SD or SEM as indicated in the figure legends. Biological sample replicates (N) are also indicated in the legends. Statistically significant differences between conditions (ΔCt values used for RT-qPCR calculations) were determined using two-tailed unpaired Student t tests or as specified in figure legends. Significance is represented as *p < 0.05, **p < 0.01, ***p < 0.001, ****p < 0.0001.

See Supplemental Experimental Procedures for additional methods.

SUPPLEMENTAL INFORMATION

Supplemental Information includes Supplemental Experimental Procedures, four figures, and two tables and can be found with this article online at http://dx.doi.org/10.1016/j.stemcr.2016.12.024.

AUTHOR CONTRIBUTIONS

L.I. and D.N.K. conceived the work and D.N.K. provided critical intellectual input. L.I. and K.D. designed experiments and wrote the manuscript. S.C. and R.S. performed experiments. A.L. performed additional RNA-seq computational analysis and generated projection scores. L.Z. performed and S.M. supervised the RNA-seq computational analysis. J.C. performed the T4 ELISA with supervision from A.N.H. T.W. characterized the iNkx2-1 cell line. L.K. engineered and characterized the plox-Nkx2-1 vector. M.K. performed gene set enrichment pathway analysis. P.M. generated the bistability model and wrote the manuscript. All authors reviewed, edited, and approved the manuscript.

ACKNOWLEDGMENTS

The targeted Ainv15 mESC line with was a kind gift from Paul Gadue (University of Pennsylvania). We would like to thank Brian R. Tilton and Patrick Autissier from the BU Flow Cytometry Core Facility as well as Michael T. Kirber from the BU Cellular Imaging Core for technical assistance. We thank Nicholas Skvir for help with visualization of RNA-seq data and Matthew Lawton for his help with immunostaining and technical assistance. K.D. was supported by a CTSI TL1 grant TL1TR001410, J.C. and A.N.H. by NIH DK105029, L.I. by NIH R01 HL111574, D.N.K. by NIH R01 HL095993, NIH R01 HL122442, and NIH DK105029, and P.M. by a Simons Investigator in MMLS (Simons Foundation).

Received: June 22, 2016
Revised: December 22, 2016
Accepted: December 23, 2016
Published: February 2, 2017

REFERENCES

Antonica, F., Kasprzyk, D.F., Opitz, R., Iacovino, M., Liao, X.H., Dumitrescu, A.M., Refetoff, S., Peremans, K., Manto, M., Kyba, M., et al. (2012). Generation of functional thyroid from embryonic stem cells. Nature *491*, 66–71.

Boggaram, V. (2009). Thyroid transcription factor-1 (TTF-1/Nkx2.1/TITF1) gene regulation in the lung. Clin. Sci. (Lond) *116*, 27–35.

Bondue, A., Lapouge, G., Paulissen, C., Semeraro, C., Lacovino, M., Kyba, M., and Blanpain, C. (2008). Mesp1 acts as a master regulator of multipotent cardiovascular progenitor specification. Cell Stem Cell *3*, 69–84.

Dravis, C., and Henkemeyer, M. (2011). Ephrin-B reverse signaling controls septation events at the embryonic midline through separate tyrosine phosphorylation-independent signaling avenues. Dev. Biol. *355*, 138–151.

Fagman, H., Amendola, E., Parrillo, L., Zoppoli, P., Marotta, P., Scarfò, M., De Luca, P., de Carvalho, D.P., Ceccarelli, M., De Felice, M., et al. (2011). Gene expression profiling at early organogenesis reveals both common and diverse mechanisms in foregut patterning. Dev. Biol. *359*, 163–175.

Ferrell, J.E. (2012). Bistability, bifurcations, and Waddington's epigenetic landscape. Curr. Biol. *22*, R458–R466.

Gadue, P., Huber, T.L., Paddison, P.J., and Keller, G.M. (2006). Wnt and TGF-beta signaling are required for the induction of an in vitro model of primitive streak formation using embryonic stem cells. Proc. Natl. Acad. Sci. USA *103*, 16806–16811.

Goss, A.M., Tian, Y., Tsukiyama, T., Cohen, E.D., Zhou, D., Lu, M.M., Yamaguchi, T.P., and Morrisey, E.E. (2009). Wnt2/2b and beta-catenin signaling are necessary and sufficient to specify lung progenitors in the foregut. Dev. Cell *17*, 290–298.

Green, M.D., Chen, A., Nostro, M.C., d'Souza, S.L., Schaniel, C., Lemischka, I.R., Gouon-Evans, V., Keller, G., and Snoeck, H.W. (2011). Generation of anterior foregut endoderm from human embryonic and induced pluripotent stem cells. Nat. Biotechnol. *29*, 267–272.

Harris-Johnson, K.S., Domyan, E.T., Vezina, C.M., and Sun, X. (2009). beta-Catenin promotes respiratory progenitor identity in mouse foregut. Proc. Natl. Acad. Sci. USA *106*, 16287–16292.

Huang, S.X.L., Islam, M.N., O'Neill, J., Hu, Z., Yang, Y.G., Chen, Y.W., Mumau, M., Green, M.D., Vunjak-Novakovic, G., Bhattacharya, J., et al. (2014). Efficient generation of lung and airway epithelial cells from human pluripotent stem cells. Nat. Biotechnol. *32*, 84–91.

Ikonomou, L., and Kotton, D.N. (2015). Derivation of endodermal progenitors from pluripotent stem cells. J. Cell Physiol. *230*, 246–258.

Ishii, J., Yazawa, T., Chiba, T., Shishido-Hara, Y., Arimasu, Y., Sato, H., and Kamma, H. (2016). PROX1 promotes secretory granule formation in medullary thyroid cancer cells. Endocrinology *157*, 1289–1298.

Kimura, S., Hara, Y., Pineau, T., FernandezSalguero, P., Fox, C.H., Ward, J.M., and Gonzalez, F.J. (1996). The T/ebp null mouse thyroid-specific enhancer-binding protein is essential for the

organogenesis of the thyroid, lung, ventral forebrain, and pituitary. Genes Dev. *10*, 60–69.

Kubo, A., Shinozaki, K., Shannon, J.M., Kouskoff, V., Kennedy, M., Woo, S., Fehling, H.J., and Keller, G. (2004). Development of definitive endoderm from embryonic stem cells in culture. Development *131*, 1651–1662.

Kurmann, A.A., Serra, M., Hawkins, F., Rankin, S.A., Mori, M., Astapova, I., Ullas, S., Lin, S., Bilodeau, M., Rossant, J., et al. (2015). Regeneration of thyroid function by transplantation of differentiated pluripotent stem cells. Cell Stem Cell *17*, 527–542.

Kyba, M., Perlingeiro, R.C.R., and Daley, G.Q. (2002). HoxB4 confers definitive lymphoid-myeloid engraftment potential on embryonic stem cell and yolk sac hematopoietic progenitors. Cell *109*, 29–37.

Lang, A.H., Li, H., Collins, J.J., and Mehta, P. (2014). Epigenetic landscapes explain partially reprogrammed cells and identify key reprogramming genes. PLoS Comput. Biol. *10*, e1003734.

Loh, K.M., Ang, L.T., Zhang, J.Y., Kumar, V., Ang, J., Auyeong, J.Q., Lee, K.L., Choo, S.H., Lim, C.Y.Y., Nichane, M., et al. (2014). Efficient endoderm induction from human pluripotent stem cells by logically directing signals controlling lineage bifurcations. Cell Stem Cell *14*, 237–252.

Longmire, T.A., Ikonomou, L., Hawkins, F., Christodoulou, C., Cao, Y.X., Jean, J.C., Kwok, L.W., Mou, H.M., Rajagopal, J., Shen, S.S., et al. (2012). Efficient derivation of purified lung and thyroid progenitors from embryonic stem cells. Cell Stem Cell *10*, 398–411.

Martin, A., Valentine, M., Unger, P., Lichtenstein, C., Schwartz, A.E., Friedman, E.W., Shultz, L.D., and Davies, T.F. (1993). Preservation of functioning human thyroid organoids in the scid mouse. 1. System characterization. J. Clin. Endocrinol. Metab. *77*, 305–310.

Mazzoni, E.O., Mahony, S., Closser, M., Morrison, C.A., Nedelec, S., Williams, D.J., An, D.S., Gifford, D.K., and Wichterle, H. (2013). Synergistic binding of transcription factors to cell-specific enhancers programs motor neuron identity. Nat. Neurosci. *16*, 1219–1286.

Millien, G., Beane, J., Lenburg, M., Tsao, P.-N., Lü, J., Spira, A., and Ramirez, M.I. (2008). Characterization of the mid-foregut transcriptome identifies genes regulated during lung bud induction. Gene Expr. Patterns *8*, 124–139.

Mou, H.M., Zhao, R., Sherwood, R., Ahfeldt, T., Lapey, A., Wain, J., Sicilian, L., Izvolsky, K., Musunuru, K., Cowan, C., et al. (2012). Generation of multipotent lung and airway progenitors from mouse ESCs and patient-specific cystic fibrosis iPSCs. Cell Stem Cell *10*, 385–397.

Oguchi, H., and Kimura, S. (1998). Multiple transcripts encoded by the thyroid-specific enhancer-binding protein (T/EBP) thyroid-specific transcription factor-1 (TTF-1) gene: evidence of autoregulation. Endocrinology *139*, 1999–2006.

Petros, T.J., Maurer, C.W., and Anderson, S.A. (2013). Enhanced derivation of mouse ESC-derived cortical interneurons by expression of Nkx2.1. Stem Cell Res. *11*, 647–656.

Pusuluri, S.T., Lang, A.H., Mehta, P., and Castillo, H.E. (2015). Cellular reprogramming dynamics follow a simple one-dimensional reaction coordinate. arXiv 1505.03889 [q-bio.MN]

Seguin, C.A., Draper, J.S., Nagy, A., and Rossant, J. (2008). Establishment of endoderm progenitors by SOX transcription factor expression in human embryonic stem cells. Cell Stem Cell *3*, 182–195.

Takahashi, K., and Yamanaka, S. (2006). Induction of pluripotent stem cells from mouse embryonic and adult fibroblast cultures by defined factors. Cell *126*, 663–676.

Ting, D.T., Kyba, M., and Daley, G.Q. (2005). Inducible transgene expression in mouse stem cells. Methods Mol. Med. *105*, 23–46.

Westerlund, J., Andersson, L., Carlsson, T., Zoppoli, P., Fagman, H., and Nilsson, M. (2008). Expression of Islet1 in thyroid development related to budding, migration, and fusion of primordia. Dev. Dyn. *237*, 3820–3829.

Xu, Q., Tam, M., and Anderson, S.A. (2008). Fate mapping Nkx2.1-lineage cells in the mouse telencephalon. J. Comp. Neurol. *506*, 16–29.

Stem Cell Reports, Volume *8*

Supplemental Information

Thyroid Progenitors Are Robustly Derived from Embryonic Stem Cells through Transient, Developmental Stage-Specific Overexpression of Nkx2-1

Keri Dame, Steven Cincotta, Alex H. Lang, Reeti M. Sanghrajka, Liye Zhang, Jinyoung Choi, Letty Kwok, Talitha Wilson, Maciej M. Kańduła, Stefano Monti, Anthony N. Hollenberg, Pankaj Mehta, Darrell N. Kotton, and Laertis Ikonomou

Figure S1

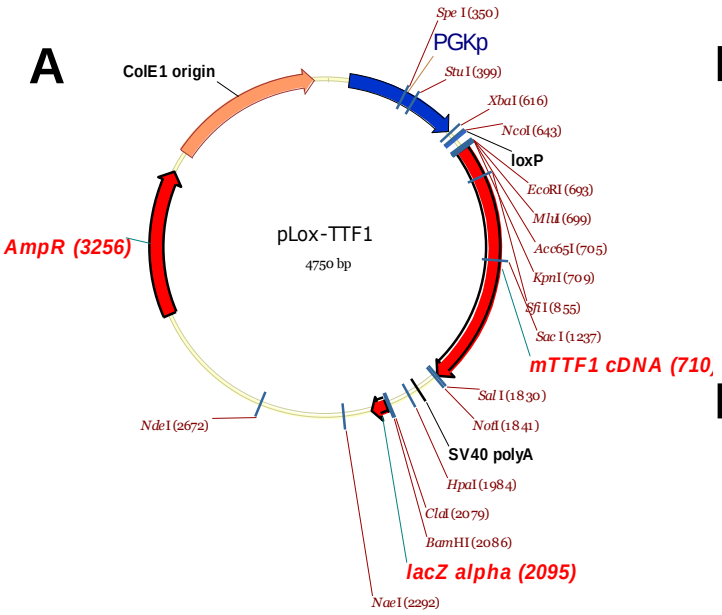
A
ColE1 origin
Spe I(350)
PGKp
Stu I(399)
Xba I(616)
Nco I(643)
loxP
EcoRI(693)
Mlu I(699)
Acc65I(705)
KpnI(709)
Sfi I(855)
Sac I(1237)
mTTF1 cDNA (710
Sal I(1830)
Not I(1841)
SV40 polyA
HpaI(1984)
ClaI(2079)
BamHI(2086)
lacZ alpha (2095)
Nae I(2292)
Nde I(2672)
AmpR (3256)
pLox-TTF1
4750 bp


B

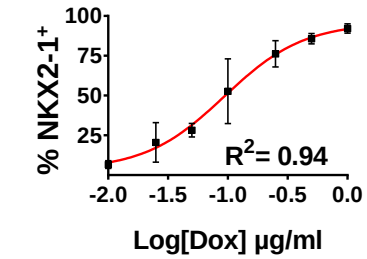
C
Dose Response
% NKX2-1+
100
75
50
25
R2= 0.94
-2.0 -1.5 -1.0 -0.5 0.0
Log[Dox] µg/ml

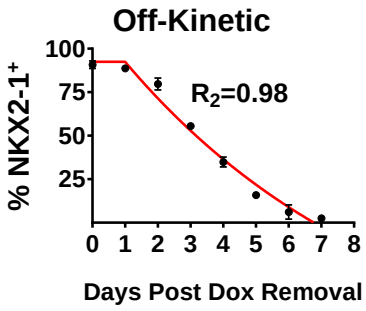
D
Off-Kinetic
% NKX2-1+
100
75
50
25
R2=0.98
0 1 2 3 4 5 6 7 8
Days Post Dox Removal

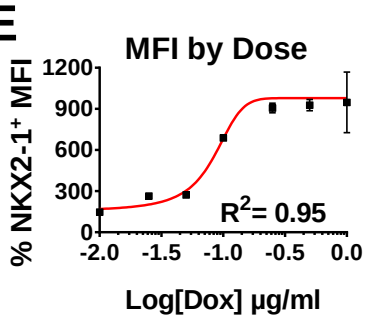
E
MFI by Dose
% NKX2-1+ MFI
1200
900
600
300
0
R2= 0.95
-2.0 -1.5 -1.0 -0.5 0.0
Log[Dox] µg/ml

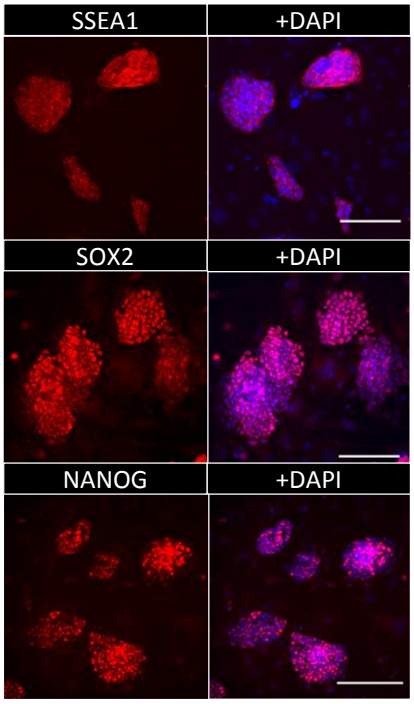
F
SSEA1
+DAPI
SOX2
+DAPI
NANOG
+DAPI

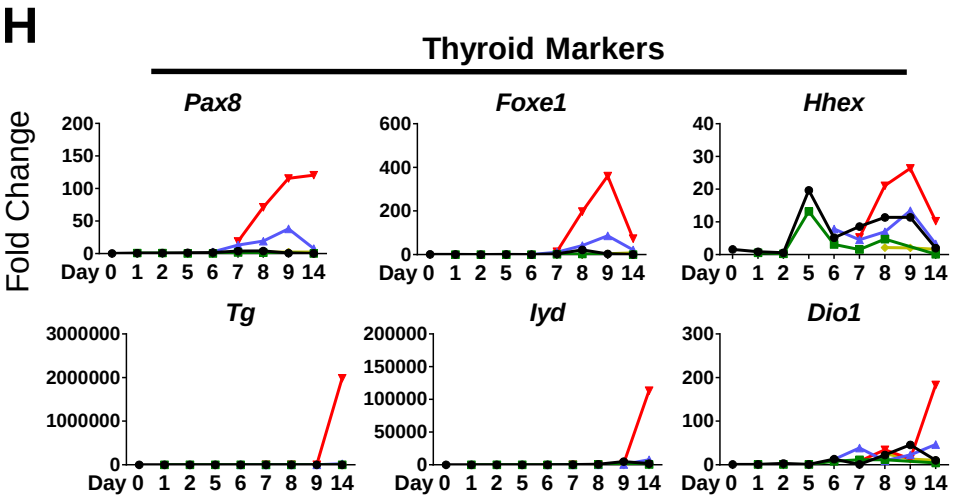
H
Thyroid Markers
Fold Change
Pax8
Foxe1
Hhex
Tg
Iyd
Dio1
Day 0 1 2 5 6 7 8 9 14

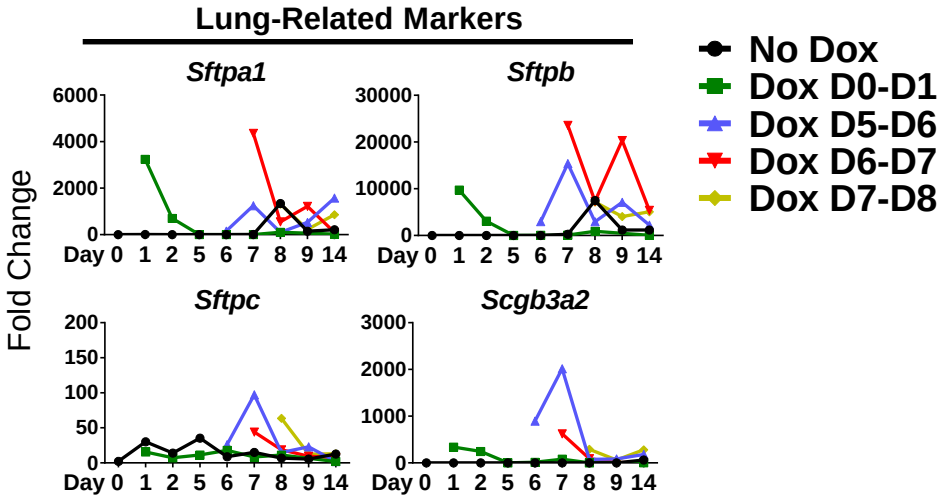
Lung-Related Markers
Fold Change
Sftpa1
Sftpb
Sftpc
Scgb3a2
Day 0 1 2 5 6 7 8 9 14
No Dox
Dox D0-D1
Dox D5-D6
Dox D6-D7
Dox D7-D8

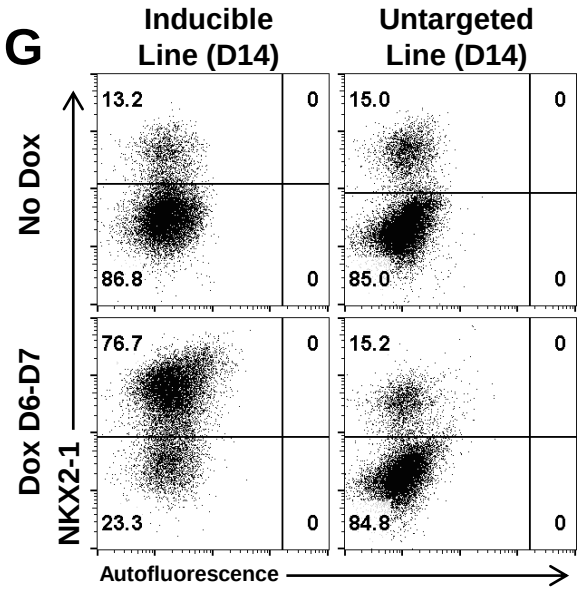
G
Inducible Line (D14)
Untargeted Line (D14)
No Dox
Dox D6-D7
NKX2-1
Autofluorescence
13.2
86.8
15.0
85.0
76.7
23.3
15.2
84.8
0

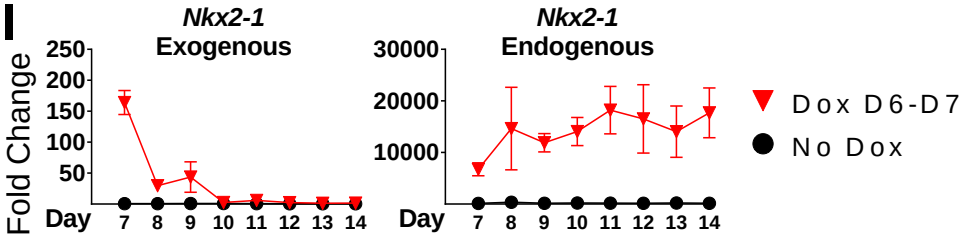
I
Nkx2-1
Exogenous
Nkx2-1
Endogenous
Fold Change
Day 7 8 9 10 11 12 13 14
Dox D6-D7
No Dox

Figure S1. (Related to Figure 1) Characterization of inducible line

(A) Plasmid map containing the Nkx2-1 transgene used to generate the iNkx2-1 line (Vector NTI graphic).

(B) Karyotyping results for the iNkx2-1 line.

(C) Dose response curve showing the percentage by flow cytometry of undifferentiated mES cells expressing NKX2-1 24 hr following a logarithmic gradient of Dox concentrations added to the media (n=2 independent experiments). Higher doses (>10 µg/ml) appeared to have a toxic effect on the cells (data not shown). A sigmoidal dose response, variable curve models the equation $Y = 3.190 + \frac{95.79-3.190}{1+10^{Log(-1.028-X)(-1.309)}}$

(D) Off kinetics of NKX2-1 expression in the iNkx2-1 line by flow cytometry following the removal of Dox from the media of undifferentiated cells (n=3 independent experiments) showing the percentage of cells steadily decreases, with virtually no remaining NKX2-1$^+$ cells after one week. The trend line models a plateau, followed by one phase decay according to the equation $Y = IF\ (x < 1,\ 92.45,\ -91.38 + (183.8)e^{-0.1211*(x-1)})$

(E) Flow cytometry median fluorescence intensity (MFI) of the NKX2-1$^+$ population, following 24 hrs of treatment with increasing doses of Dox. The MFI of the NKX2-1$^+$ population was consistently high above 0.1 µg/ml of Dox, indicating the effect of the Dox regulates the percentage of NKX2-1$^+$ cells and not the amount of expression per cell.

(F) Immunostaining for markers of pluripotency in undifferentiated iNkx2-1 mES colonies. Scale bar represents 200 µm.

(G) D14 flow cytometry from parallel differentiations using the parent untargeted line and the targeted inducible line with and without Dox addition D6-D7.

(H) Time course of thyroid and lung marker gene expression by RT-qPCR following individual 24-hr pulses of Dox treatments at specific stages of the directed differentiation protocol. Fold changes are calculated relative to D0 undifferentiated cells, error bars represent SD (n=3 independent experiments).

(I) Time course of exogenous and endogenous Nkx2-1 expression following Dox treatment from D6-D7. Error bars represent SEM from three independent experiments

Figure S2

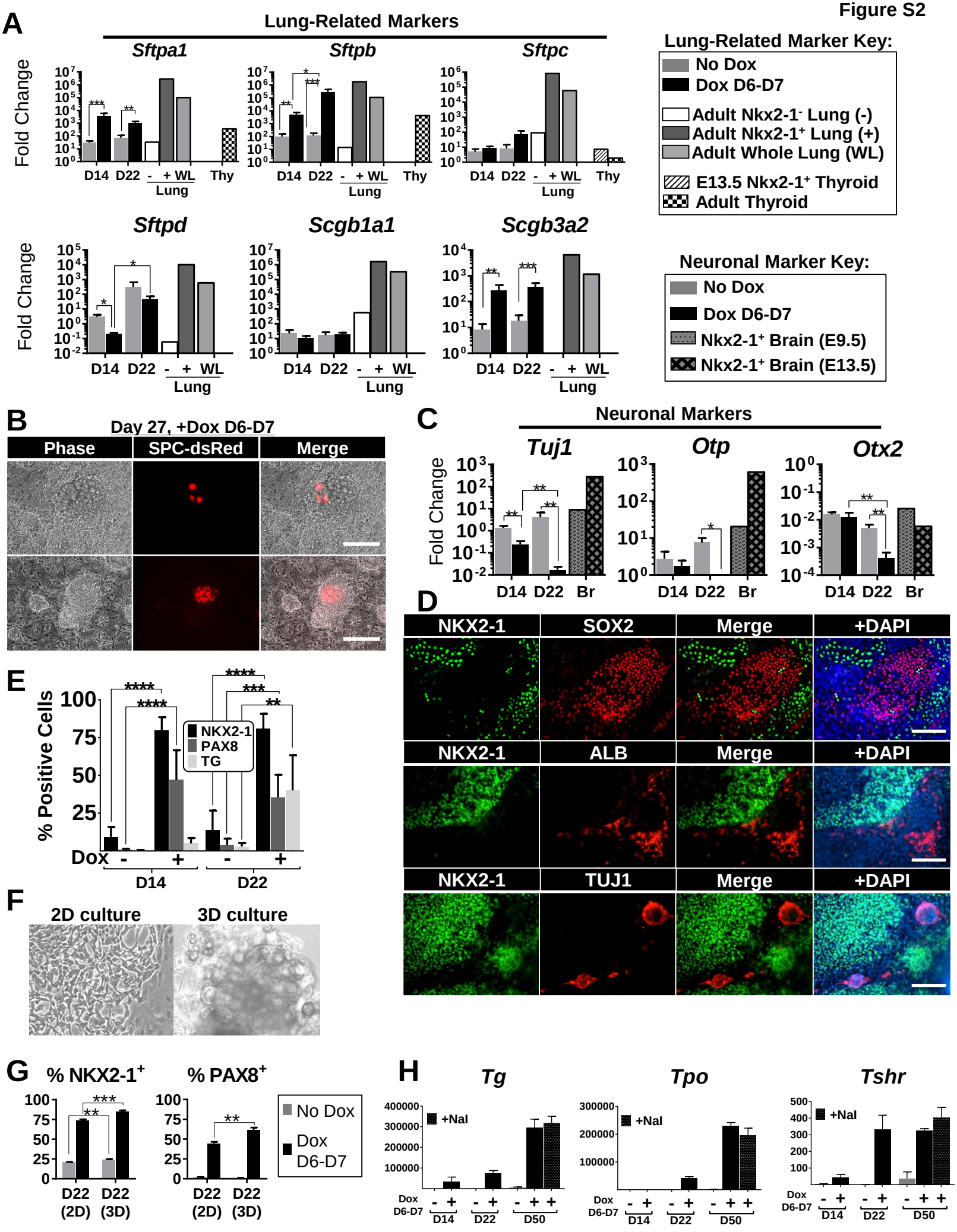
A
Lung-Related Markers
Sftpa1
Sftpb
Sftpc
Sftpd
Scgb1a1
Scgb3a2
Fold Change
D14 D22 - + WL Lung Thy
Lung-Related Marker Key:
No Dox
Dox D6-D7
Adult Nkx2-1- Lung (-)
Adult Nkx2-1+ Lung (+)
Adult Whole Lung (WL)
E13.5 Nkx2-1+ Thyroid
Adult Thyroid
Neuronal Marker Key:
No Dox
Dox D6-D7
Nkx2-1+ Brain (E9.5)
Nkx2-1+ Brain (E13.5)
B
Day 27, +Dox D6-D7
Phase
SPC-dsRed
Merge
C
Neuronal Markers
Tuj1
Otp
Otx2
Fold Change
D14 D22 Br
D
NKX2-1
SOX2
Merge
+DAPI
NKX2-1
ALB
Merge
+DAPI
NKX2-1
TUJ1
Merge
+DAPI
E
% Positive Cells
NKX2-1
PAX8
TG
Dox - + - +
D14 D22
F
2D culture
3D culture
G
% NKX2-1+
% PAX8+
D22 (2D) D22 (3D)
No Dox
Dox D6-D7
H
Tg
Tpo
Tshr
+Nal
Dox D6-D7 - + - + - + +
D14 D22 D50

Figure S2. (Related to Figure 2) Nkx2-1 overexpression at AFE stage results in efficient thyroid differentiation

(A) Gene expression by RT-qPCR of lung markers in the Dox-treated (D6-D7) and untreated conditions (n=5 independent experiments). Controls are FACS purified Nkx2-1$^{GFP+/-}$ lung populations and whole lung from an adult Nkx2-1^{GFP} reporter mouse, as well as E13.5 Nkx2-1^{GFP+} thyroid and adult thyroid,. Fold changes are calculated relative to D0 undifferentiated cells, error bars represent SEM (n=5 independent experiments).

(B) Cells transduced with the SPC-dsRed reporter lentivirus show minimal induction of the lung alveolar marker SPC by D27. Scale bars represents 100 µm.

(C) Gene expression by RT-qPCR of neuronal markers in the Dox-treated (D6-D7) and untreated conditions (n=5 independent experiments). Controls are FACS purified E9.5, E13.5 Nkx2-1^{GFP+} forebrain cells. Fold changes are calculated relative to D0 undifferentiated cells, error bars represent SEM (n=5 independent experiments).

(D) Immunostaining of D14 Dox-treated (D6-D7) conditions shows non-overlap of NKX2-1 with SOX2 (endodermal or lung lineage marker), ALB (liver marker) and TUJ1 (neural marker). Scale bars represent 100 µm.

(E) Percent positive populations of NKX2-1, PAX8, TG quantified by flow cytometry. Error bars represent SD (n=4 independent experiments).

(F) Phase contrast micrographs showing the cell morphology at D22 of cells grown on two-dimensional gelatin coated plates (left panel) or embedded in three-dimensional Matrigel from D14-D22 (right panel).

(G) Flow cytometry quantification of intracellular staining for NKX2-1^{+} and PAX8^{+} cells grown in 2D vs. 3D culture conditions (n= 3 wells from the same differentiation).

(H) Gene expression data of cells cultured to D50 for T4 ELISA analysis as in Figure 2D,E (n=3 wells from the same differentiation).

Figure S3

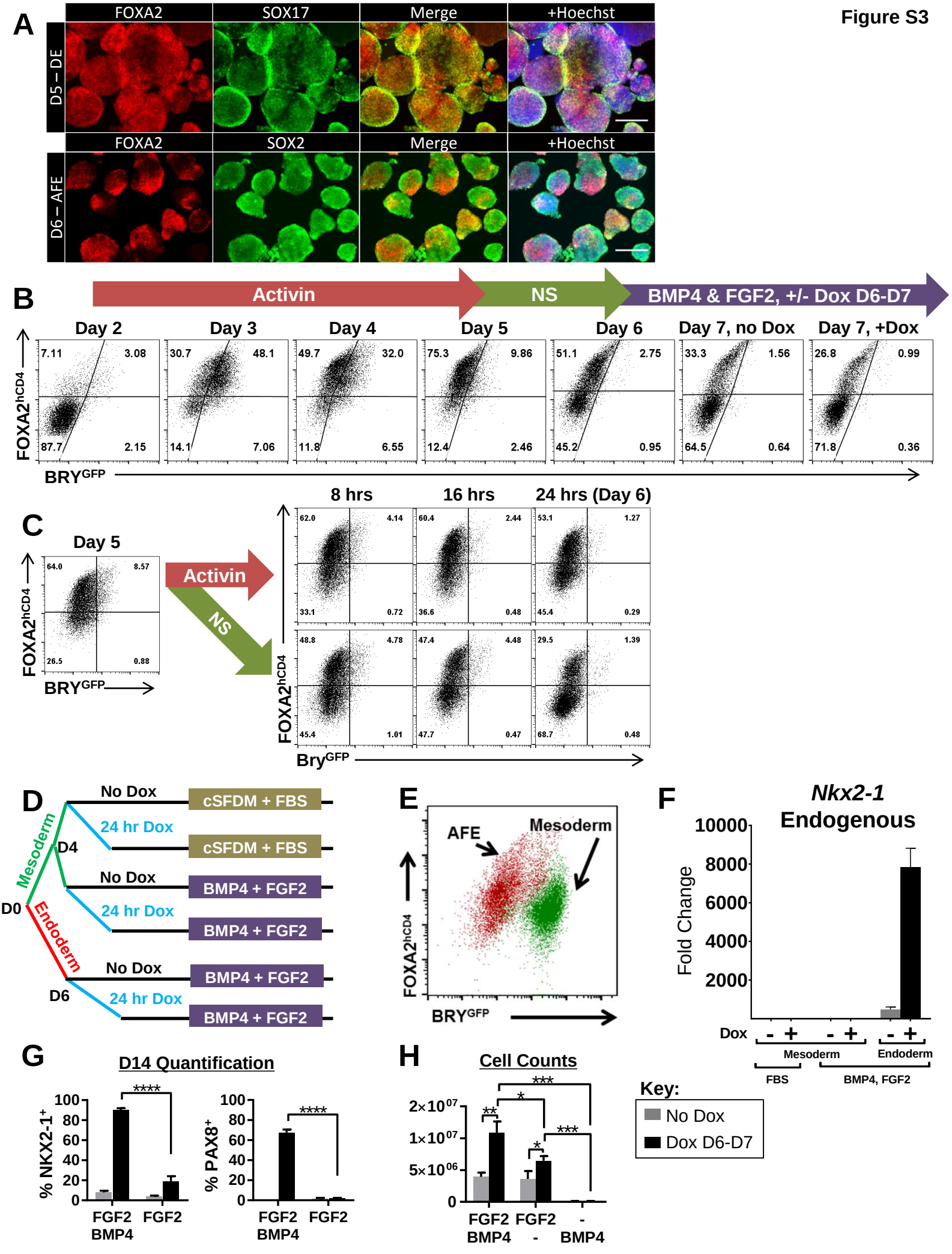
A
FOXA2
SOX17
Merge
+Hoechst
D5 – DE
FOXA2
SOX2
Merge
+Hoechst
D6 – AFE
B
Activin
NS
BMP4 & FGF2, +/- Dox D6-D7
Day 2
Day 3
Day 4
Day 5
Day 6
Day 7, no Dox
Day 7, +Dox
FOXA2hCD4
BRYGFP
C
Day 5
Activin
NS
8 hrs
16 hrs
24 hrs (Day 6)
FOXA2hCD4
BryGFP
D
No Dox
24 hr Dox
cSFDM + FBS
BMP4 + FGF2
Mesoderm
Endoderm
D0
D4
D6
E
AFE
Mesoderm
FOXA2hCD4
BRYGFP
F
Nkx2-1
Endogenous
Fold Change
Dox
Mesoderm
Endoderm
FBS
BMP4, FGF2
G
D14 Quantification
% NKX2-1+
% PAX8+
FGF2
BMP4
H
Cell Counts
Key:
No Dox
Dox D6-D7

Figure S3. (Related to Figure 3) Efficient specification is dependent on precise modulation of BMP/FGF signaling and derivation of the thyroid-competent Foxa2Neg AFE population

(A) Endoderm staining for markers of DE and AFE show efficient derivation. Scale bars represent 200 μm.

(B) Flow cytometry data showing the induction kinetic of $Foxa2^{+}$ definitive endoderm, stained using the hCD4 knock-in reporter. Using the $Foxa2^{hCD4}$ and Bry^{GFP} reporters we were able to track the DE derivation through an anterior primitive streak (double positive) intermediate. When cells are hereafter exposed to NS treatment, expression of FOXA2 by percentage rapidly decreases during this 24 hr period, resulting in two populations ($FOXA2^{High}$ and $FOXA2^{Neg}$).

(C) D5-D6 $FOXA^{hCD4}$ kinetic (NS media vs. Activin). When cells remain in Activin in place of the NS treatment, loss of FOXA2 does not occur to the same extent, indicating this drop is in response to the NS treatment.

(D) Experimental schematic of AFE vs. mesodermal population derivation and media used for specification and outgrowth. Early mesoderm at D4 ("Mesoderm" branch) was cultured +/- Dox for 24 hrs, either in mesoderm-promoting media (DMEM+FBS) or in the thyroid specification media (BMP4/FGF2) for comparison to the thyroid protocol ("Endoderm" branch), also +/- Dox D6-D7.

(E) Flow cytometry comparison of FOXA2, BRY expression in AFE vs. mesodermal stage populations.

(F) RT-qPCR for endogenous Nkx2-1 expression for the conditions described in (E), duplicate samples. Fold changes were calculated relative to D0 undifferentiated cells.

(G) Flow cytometry quantification at D14 of $NKX2\text{-}1^{+}$ and $PAX8^{+}$ cells from cultures grown (as in Fig 3G) with both specification factors compared to FGF2 alone. Error bars represent SD of biological triplicates within the same differentiation

(H) Cell counts (cells/well of a 6-well plate) harvested at D14 (same conditions as in G).

A

RNA-Seq Data:
Gene Ontology in Sample Sets

Figure S4

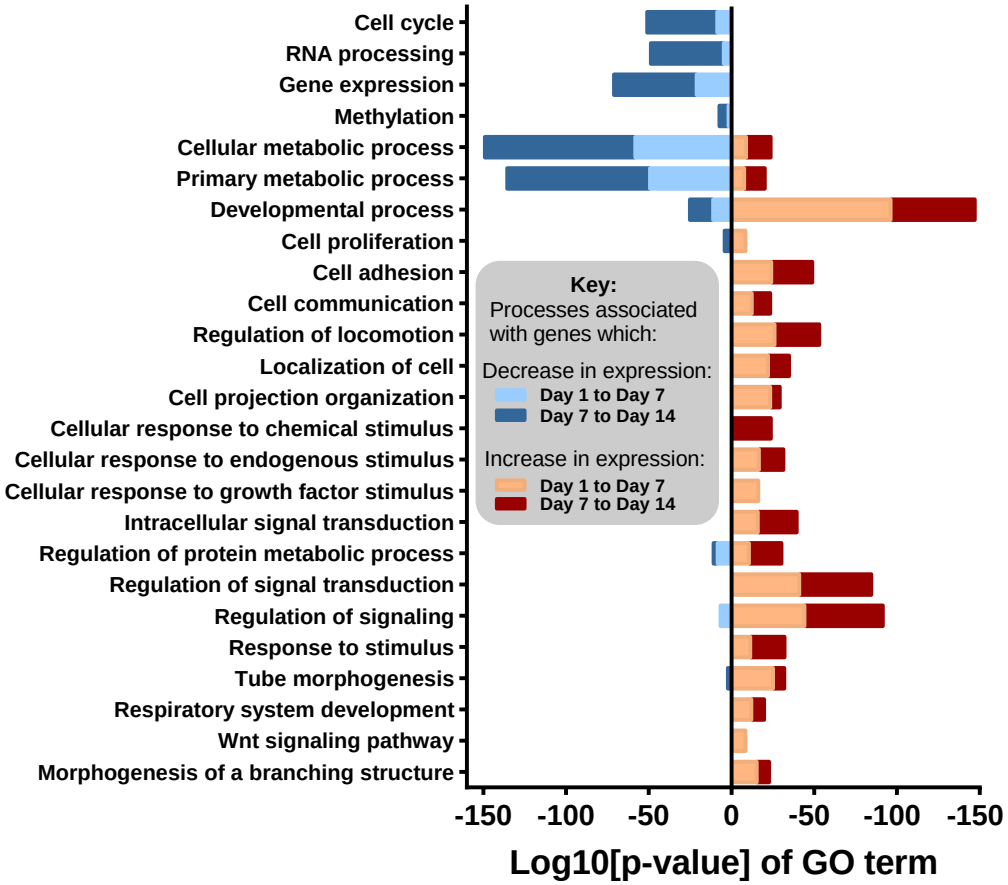

B

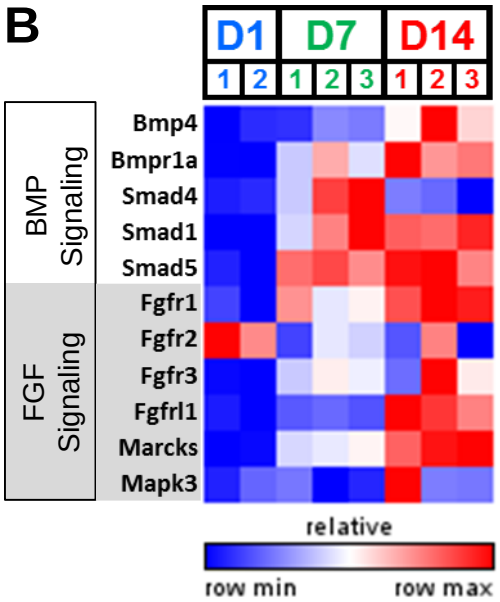

C

"Late" Cluster GSEA Analysis	
Enriched GO Molecular Functions	**FDR q-val**
SEQUENCE-SPECIFIC DNA BINDING TRANSCRIPTION FACTOR ACTIVITY	1.80E-02
GROWTH FACTOR ACTIVITY	1.81E-02
COLLAGEN BINDING	2.46E-02
SEQUENCE-SPECIFIC DNA BINDING	4.07E-02
ION CHANNEL ACTIVITY	4.14E-02
CALCIUM ION BINDING	5.64E-02
HEPARIN BINDING	6.22E-02
PROTEIN HETERODIMERIZATION ACTIVITY	6.58E-02
METALLOENDOPEPTIDASE ACTIVITY	6.95E-02
PROTEIN HOMODIMERIZATION ACTIVITY	7.71E-02
RNA POLYMERASE II CORE PROMOTER INVOLVED IN POSITIVE REGULATION OF TRANSCRIPTION	7.77E-02
G-PROTEIN COUPLED RECEPTOR ACTIVITY	1.31E-01
IDENTICAL PROTEIN BINDING	1.44E-01
TRANSMEMBRANE SIGNALING RECEPTOR ACTIVITY	1.59E-01
METALLOPEPTIDASE ACTIVITY	1.76E-01
DNA BINDING	1.83E-01
Enriched KEGG Pathways	**FDR q-val**
PROTEIN DIGESTION AND ABSORPTION	0.00E+00
NEUROACTIVE LIGAND	0.00E+00
ECM-RECEPTOR INTERACTION	2.89E-03
CYTOKINE-CYTOKINE RECEPTOR INTERACTION	3.19E-02
PI3K-AKT SIGNALING PATHWAY	7.35E-02
PURINE METABOLISM	1.05E-01

D

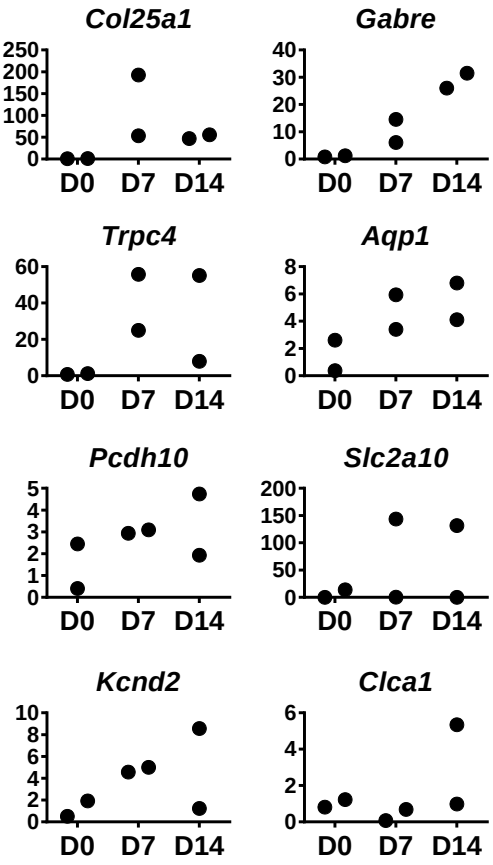

E

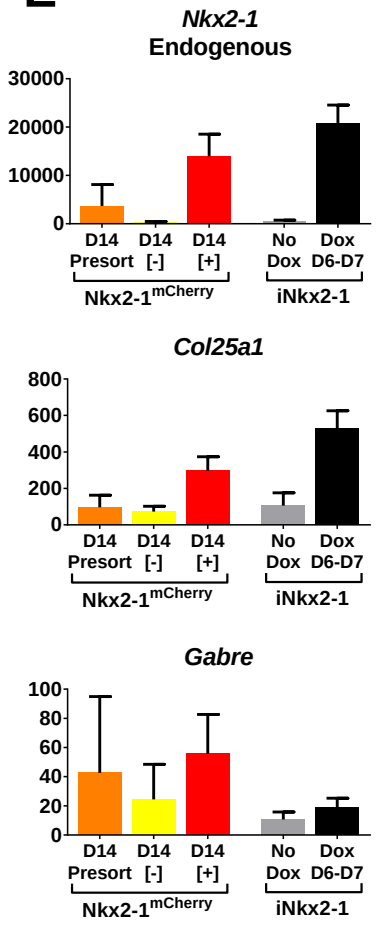

Figure S4. (Related to Figure 4) RNA-Sequencing data reveals thyroid developmental processes

(A) Functional Analysis: Gene Ontology processes associated with genes with significant differential expression ($P<0.05$) between time points. Terms shown represent relevant biological processes of interest. Bars represent differentially expressed processes between conditions, full length of each bar is the combined value (stacked) of both sets.

(B) Differential gene expression from RNA-Seq of selected genes involved in BMP and FGF signaling.

(C) GSEA pathway analysis of the "Late" cluster gene set.

(D) RT-qPCR validation data of cell surface markers identified in the "Late" cluster (n=2 independent experiments).

(E) Further gene expression analysis of select targets from (G) with purified Nkx2-1$^{mCherry+}$ from the thyroid protocol for validation (n=3 independent experiments).

Supplemental Tables

Table S1. Related to Figure 4. Transcription factors from the "Early" and "Late" clusters identified from RNA-Sequencing (GEO accession number GSE92572**).** Relative gene expression across samples, low (blue) to high (red), is indicated.
[a]Genes referenced in Longmire et al.
[b]Genes referenced in Millien et al.
[c]Genes referenced in Fagman et al.

Table S2. Related to Figure 4. Putative cell surface markers factors from the "Early" and "Late" clusters identified from RNA-Sequencing (GEO accession number GSE92572**).** Relative gene expression across samples, low (blue) to high (red), is indicated.
[a]Genes referenced in Longmire et al.
[c]Genes referenced in Fagman et al.

Supplemental Experimental Procedures:

mESC Maintenance

Undifferentiated mESCs were maintained on a feeder layer of mitotically inactivated mouse embryonic fibroblasts (MEFs) in serum-containing media consisting of DMEM (Life Technologies, 11995-073) with 15% FBS (Thermo Fisher Scientific, NC0712155), 200 mM L-glutamine (Invitrogen, 25030-164) and 100 µg/ml Primocin (Thermo Fisher Scientific, NC9392943), supplemented with LIF-containing conditioned media (Millipore, ESG1106) at 1 U/ml or an equivalent concentration of conditioned LIF produced in our lab. mESCs were passaged as needed when cultures reached appropriate confluency using 0.05% trypsin (Invitrogen, 25300-120) for continued expansion on MEFs or to start differentiation experiments. ESCs or differentiated cells were counted using the Countess II Automated Cell Counter (Thermo Fisher Scientific, AMQAX1000) according to the manufacturer's instructions.

Karyotype Analysis

Cytogenetic analysis (Cell Line Genetics) was performed on twenty G-banded metaphase cells from the chosen mESC line. The majority (18/20) cells demonstrated an apparently normal male karyotype, while two cells demonstrated loss of the Y chromosome (Figure S1B), a common feature of cultured mouse ESCs. Cells were expanded for a minimal (≤4) number of passages before being used in experiments to avoid genetic instability.

Mouse ESC Directed Differentiation

To initiate directed differentiation, ESC colonies cultured on mouse embryonic fibroblasts (MEFs) were trypsinized to form a single cell suspension and MEFs were depleted for 30 min at 37ºC in mESC media on a tissue culture dish. The supernatant containing the ESCs was rinsed and cells were transferred at a density of 500,000 cells per 10 cm petri dish into complete serum-free differentiation media (cSFDM) containing 75% IMDM (Life Technologies, 12440061) and 25% Ham's Modified F12 medium (Thermo Fisher Scientific, MT-10-080-CV) supplemented with N2 (Life Technologies, 17502-048), B27 with RA (Life Technologies, 17504-044), 0.05% BSA (Life Technologies, C15260-037), 2 mM L-glutamine (Invitrogen 25030-164), 0.05 mg/ml ascorbic acid (Sigma A4544-25G), $4.5x10^{-4}$M monothioglycerol (MTG) (Sigma M6145) and 100 µg/ml Primocin (Fisher NC9392943). Cells were grown in this media for 48 hours, where they formed embryoid bodies (EBs). At day 2, EBs were monodispersed by trypsinization and cells were re-suspended in cSFDM containing 50 ng/ml Activin A (R&D systems 338-AC) to re-form EBs and induce definitive endoderm. After 72 hrs of Activin A exposure, endoderm induction was confirmed by expression of Foxa2-hCD4 by flow cytometry (Gadue et al., 2006; Gouon-Evans et al., 2006). EBs were rinsed with base media and transferred to anteriorization media containing cSFDM supplemented with 100 ng/ml Noggin (Fisher Scientific, 1967-NG-025) and 10 µM SB431542 (Fisher, 16-141-0) for BMP and TGFβ inhibition. After 24 hr exposure to these factors, EBs were trypsinized for monodispersion and plated at a density of 200,000 cells per 9.5 cm^2 onto gelatin-coated cell culture dishes (Corning Costar, 3516 or 3513). Plating EBs or monodispersed cells at this time point did not significantly affect Nkx2-1 induction or thyroid specification (data not shown). Specification media from day 6 to day 14 consisted of cSFDM supplemented with 10 ng/ml hBMP4, 250 ng/ml rhFGF2 (R&D Systems, 233-FB-01M) and 100 ng/ml Heparin Sodium Salt (Sigma Aldrich H3149-100KU) (Kurmann et al., 2015). Upon initial plating at day 6, ROCK inhibitor (Y27632, TOCRIS 1254) was added to the media until day 7 to aid in survival of monodispersed cells. Dox (Doxycycline Hyclate, Sigma, D9891-5G) was added to treated conditions as indicated at a concentration of 1 µg/ml and removed after 24 hr by rinsing cultures twice with basal media and replacing with Dox-free specification media. Media was replaced as needed until day 14, when cells were harvested for analysis or passaged to day 22 or later for further expansion and maturation in cSFDM supplemented with 250 ng/ml rhFGF2, 100 ng/ml rhFGF10 (R&D 345-FG), and 100 ng/ml Heparin Sodium Salt (FGF2+10 media). As indicated in the text, these day 14 cells were either passaged onto gelatin-coated tissue culture plates at a density of about 21,000 cells/cm^2 or mixed into undiluted growth factor reduced Matrigel drops (Corning, 356231) at a density of 80,000 cells per 100 µl. At day 22 or 30, cells were harvested for analysis as described in the following analysis subsections.

For extended maturation to day 50, cells were grown and plated into Matrigel droplets at day 14 as described above and subsequently cultured as previously described (Kurmann et al., 2015). Media from D14-22 consisted of cSFDM supplemented with 250 ng/ml rhFGF2, 100 ng/ml rhFGF10, 100 ng/ml Heparin Sodium Salt, 1 mU/ml bTSH (Los Angeles Biomedical Research Institute National Hormone & Peptide Program, AFP-8755B), 25 ng/ml rhEGF (R&D Systems, 236-EG), 50 ng/ml IGF1 (R&D Systems, 791-MG), and 10 µg/ml Insulin (Sigma, 10516-5ml). Media from D22-D30 consisted of cSFDM supplemented with 250 ng/ml rhFGF2, 100 ng/ml rhFGF10, 100 ng/ml Heparin Sodium Salt, 1 mU/ml bTSH, 25 ng/ml rhEGF, 50 ng/ml rmIGF1, and 5 µg/ml ITS (Thermo Fisher Scientific, 41400045). Media from D30-D50 consisted of Ham's Modified F12 medium supplemented with 10 mM HEPES (Sigma H0887), 0.25% BSA, 0.8 mM $CaCl_2$ (Sigma, C1016), 50 nM Dexamethasone (Sigma, D4902), 100 ng/ml

Heparin Sodium Salt, 1 mU/ml bTSH, 25 ng/ml rhEGF, 50 ng/ml rmIGF1, and 5 μg/ml ITS. NaI (Sigma-Aldrich, 383112) was added at a concentration of 10 μM from D40-D50.

Directed differentiation to mesoderm consisted of a two day LIF depletion in cSFDM to allow formation of EBs, followed by two days mesoderm induction with 2 ng/ml Activin A, 3 ng/ml hBMP4, and 0.3 ng/ml rmWnt3a (R&D Systems, 1324-WN). For the purpose of experiments described, cultures at day 6 (endoderm) or day 4 (mesoderm) were plated either into thyroid specification media (FGF2+BMP4 as described above) or mesodermal outgrowth media (cSFDM supplemented with 20% FBS). Cultures were treated with Dox for 24 hrs in parallel to untreated cultures, and analyzed after 8 days of outgrowth.

Immunostaining

2-Dimensional culture: Samples were grown from day 6 to day 14 or 22 (passaged on day 14) on gelatin-coated tissue culture dishes and fixed in 4% paraformaldehyde (PFA) (Ted Pella, 18505) for 15 minutes, then rinsed twice with PBS and stored at 4ºC if staining was not performed the same day. Cells were permeabilized with 0.2% Triton X-100 detergent (Thermo Fisher Scientific, 28314) in PBS for five minutes, rinsed twice, and then blocked with 1% BSA in PBS for 30 minutes. The samples were then incubated with the primary antibody in 1% BSA at dilutions listed below overnight at 4ºC. Pax8 and Tg antibodies were blocked in 1% BSA with 0.1% Triton X. Fluorophore-conjugated secondary antibodies were added at the concentrations listed below and incubated for one hour at 37ºC and rinsed twice with PBS. To counterstain nuclei, cultures were incubated for 5 min with 1 μg/ml DAPI (Life Technologies, D1306) or 500 nM PI (Life Technologies P3566). Cultures were rinsed twice with PBS and stored in PBS at 4ºC until imaged.

3-Dimensional culture: Cells were grown on gelatin-coated tissue culture dishes from day 6 to day 14, and then passaged into undiluted Matrigel where they were grown until day 22 or 30. Matrigel was dissolved using 2 mg/ml Dispase (Invitrogen 17105-041) in DMEM incubated at 37ºC for 30 min, or Cell Recovery Solution (Corning CB-40253) added for 1 hr at 4ºC. The resulting free-floating cell structures were fixed in 4% PFA for 15 minutes, and rinsed twice with PBS. Cells were then embedded into agarose (Sigma, A9414) melted at 67ºC, and cooled at 4ºC or on ice for at least one hour. The agar/cell pellets were then processed into paraffin similar to a tissue sample using standard paraffin embedding procedures. For staining, slides were deparaffinized and steamed for 30 min in Target Retrieval Solution (Dako, S1699). Individual sections on slides were segregated using a PAP pen (Abcam, ab2601) and were blocked with 1% BSA in PBS for 30 minutes. The samples were then incubated with the primary antibody in 1% BSA at dilutions listed below overnight at 4ºC. The next day, slides were rinsed twice in PBS and incubated with fluorophore-conjugated secondary antibodies for one hour at 37ºC followed by two rinses with PBS. Cells sectioned onto slides were mounted with either SlowFade Diamond Antifade with DAPI (Life Technologies, S36964) or were counterstained with DAPI or Hoechst (Life Technologies, H3570) at 20 μg/ml for 10 min and subsequently mounted with Prolong Diamond Antifade Mountant (Life Technologies, P36961), sealed the following day, and stored at 4ºC until imaging.

Primary Antibodies						
Protein Target	**Company**	**Catalog Number**	**Host Species**	**Clonality**	**Dilution: Flow Cyt.**	**Dilution: ICC/IHC**
NKX2-1	Dako	M3575	Mouse	monoclonal		1:200
NKX2-1	Abcam	ab76013 (Isotype ab172730)	Rabbit	monoclonal	1:50	1:200
PAX8	Abcam	ab122944 (Isotype: ab172730)	Rabbit	monoclonal		1:200
PAX8	Biocare	ACI438C (Isotype: NC490)	Mouse	monoclonal	1:50	1:200
TG	Abcam	ab80783	Mouse	monoclonal	1:50	1:200
ECAD	Abcam	ab76319	Rabbit	monoclonal		1:100
ALB	Dako	A0001	Rabbit	polyclonal		1:1000
TUJ1	Sigma	T2200	Rabbit	polyclonal		1:1000
SSEA1	Millipore	90230	Mouse	monoclonal		1:50
NANOG	Abcam	Ab80892	Rabbit	polyclonal		1:50
T4	Thermo Scientific	MA5-14716	Mouse	monoclonal		1:100

NIS	Imanis Life Sciences	REA008	Rabbit	polyclonal		1:2000
FOXA2	Abcam	Ab108422	Rabbit	monoclonal		1:300
SOX17	R&D Systems	AF1924	Goat	polyclonal		1:50
SOX2	BD Pharmingen	561469	Mouse	monoclonal		1:100
hCD4	Life Technologies	MHCD0404 (Isotype: MG2A04)	Mouse (RPE)	monoclonal	1:10	
SIRPA	BD Biosciences	560107 (Isotype: 553925)	Rat (PE)	monoclonal	1:50	
EPHB2	BD Biosciences	564699 (Isotype: 550854)	Mouse (APC)	monoclonal	1:50	
Secondary Antibodies						
Alexa Fluor 488	Invitrogen	A10667	goat anti mouse		1:100	1:300
DyLight 550	Abcam	ab96884	goat anti-rabbit			1:300
Alexa Fluor 647	Invitrogen	A21245	goat anti-rabbit		1:100	

Image Acquisition

Fluorescent micrographs were acquired on the Nikon Eclipse T*i* inverted microscope (Boston University Cellular Imaging Core) or a Nikon Eclipse N*i* upright microscope using the NIS-Elements software. Acquired ND2 files were processed with Fiji (Schindelin et al., 2012; Schneider et al., 2012) to optimize clarity and create merged micrographs. Large-scale composite micrographs (Fig. S3) were acquired using the Nexcelom Celigo Cyntellect Imaging Cytometer microwell plate imager.

Phase contrast micrographs and phase contrast / fluorescent micrographs were acquired using a Nikon Eclipse TS100 (Diagnostic Instruments Inc., Model #18.2 Color Mosaic) microscope with a Lumen200 Fluorescent Illumination (Prior Scientific) and the SPOT Insight Firewire 2 camera (Diagnostic Instruments Inc., Model 18.2) and the SPOT Software Version 4.6.1.38.

Real-Time Quantitative Polymerase Chain Reaction (RT-qPCR)

To harvest cells, cultures on tissue culture dishes were rinsed and trypsinized with 0.05% trypsin until dissociated. FBS (Fisher, SH3007003E) was added to quench enzymatic activity, and cells were rinsed with basal media (DMEM) and centrifuged to pellet. Cell pellets were stored at -80ºC until ready for processing.

RNA was extracted using QIAshredder columns (QIAGEN, 79656) and the RNeasy Plus Mini Kit (QIAGEN, 74136) according to the QIAGEN manual instructions. Purified RNA was eluted in 30 µl nuclease-free water, quantified on the Nanodrop (ND1000), and diluted as needed. cDNA was prepared using Taqman Reverse Transcription Reagents (Applied Biosystems, N808-0234). cDNA samples were prepared with TaqMan Fast Universal Master Mix (Life Technologies, 4367846) and diluted to 6.25 ng per 25 µl reaction for real-time analysis on the StepOnePlus Real Time PCR System (Applied Biosystems). Relative expression analysis calculations were performed according to the ΔΔCT method (Livak and Schmittgen, 2001) utilizing 18S rRNA as the internal reference gene and undifferentiated ESCs collected prior to each differentiation as the reference sample. If expression was undetected based on the set threshold, the value was set to the maximum number of cycles (40) to allow fold change calculations. Data was graphed for visualization as shown in the figures using the GraphPad Prism 6 software.

Custom probes specific for endogenous and exogenous Nkx2-1 were designed using the Custom Taqman Assay Design Tool. Sequences were entered that spanned the transgene to the 3' UTR to create the endogenous specific probe, and the transgene to the polyA tail of the transgene to create the exogenous specific probe.

Initial validation for the RNA-Sequencing was performed using Custom TaqMan Array Plates, 96 well format (Thermo Fisher Scientific, 4413255, "Early" cluster Design ID: PPFGSW4, "Late" cluster Design IDs: PP4FSDO, PP5OQJW).

RT-qPCR Taqman Probes		
Expression Target	**Company**	**Catalog Number**
18S rRNA	Thermo Fisher	4319413e
Endogenous Nkx2-1	Thermo Fisher	4441117 Assay ID: AJLJIJO
Exogenous Nkx2-1	Thermo Fisher	4331348 Assay ID: AIVI6DF
Pax8	Thermo Fisher	Mm00440623_m1

Tg	Thermo Fisher	Mm00447525_m1
Foxe1	Thermo Fisher	Mm00433948_m1
Hhex (Hex1)	Thermo Fisher	Mm00433954_m1
Slc5a5 (Nis)	Thermo Fisher	Mm00475074_m1
Tpo	Thermo Fisher	Mm00456355_m1
Tshr	Thermo Fisher	Mm00442027_m1
Iyd	Thermo Fisher	Mm00503564_m1
Dio1	Thermo Fisher	Mm00839358_m1
Sftpa (Spa)	Thermo Fisher	Mm00499170_m1
Sftpb (Spb)	Thermo Fisher	Mm00455681_m1
Sftpc (Spc)	Thermo Fisher	Mm00488144_m1
Scgb3a2	Thermo Fisher	Mm00504412_m1
Trp63 (P63)	Thermo Fisher	Mm00495788_m1
Scgb1a1 (Cc10)	Thermo Fisher	Mm00442046_m1
Abca3	Thermo Fisher	Mm00550501_m1
Col25a1	Thermo Fisher	Mm00472589_m1
Gabre	Thermo Fisher	Mm00489935_m1

Target sequence of *Nkx2-1* 3' UTR used to design the *Nkx2-1* endogenous-only probe:
GTTCTACCTTGCTTTATGGTCGGACCTGGTGAGACGTGAGATGCGCTTGA
GCCCCGCGCGACCTCAACGCTTCCCCTCTGCCTTCCGCAAAGACCACCAT
TCGCCCGCTGCTCCACGCGCTTCTACTTTTTTTAAGAATCTGTTTATGTT
TAGACCAAGGAAAAGTACACAAAGACCAAACTGCTGGACGACTTCTTCTT
CTTCTTCTTCTTCTTCTTCTTCTTCTTCTTCTTCTTCTTCTTCTTCTCT
TCTTCTTCTTCTTCTTCTTCTTCTTCTCCTCCTCCTCCTCCTCCTCC
TCCTCCTCCTCCTCTTCCTCCTTCTTGTCCCCGCTCGTTCTTTTCTTTCT
CCCCCTCCTCTTCTGTTTCCTTCTTCCTTCATCTTTCCCCCCTTCCTTTC
TCTTTACTATCTAAAACTTGCAGACTTTTTGTTTTTTAACATAAAAAGAA
AATAGAAACAGCCAAGCAAATTCAACCCTTTACGGATTCTTTAAACAGAG
AAGGACAGAGAACAAATTTGGGGTGTCTTTCTGGTAGTTCAAATGGGTTC
CCAAGCTTAGGCATGGCACAGTTTTGGAGCCTGTTCTATGCTTCCATGGC
CCTGAACTCTAAAGACGGAAAACTTTTCTGTGGATGCACCCTGCCAGCAA
AGTGAGCTTGCTTGTAAATACCAGGATTTTTCGTTTGTTTGTATGTTTCA
GAAGGGAGGACAGACGCTGGAGATAGGAAAGTCTTCAGCATAACCCATTT
GTACCTGACACAAAGGAAGTGTCCCCTCCCAGGCGCCCTCTGGCCCTACA
GGTTCAGTCCAGGCTGGCCTTTCAGAAAATTGTTTTAGGTTTGATGTGAA
CTTGTAGCTGTAAAATGCTGTTAAAAGTTGGACTAAATGCCTAGTTTTTA
GTAACCTGTACATTATGTTGTAAAAAGAACCCCAGTCCCAGTCCCTAGTC
CCTCACTTTTTCAAGGGGCATTGACAAACCTGTGTATATTATTTGGCAGT
TTGGTATTTGCAGCACCAATCCTTTTTTTTTTTCTGTTGTAACTTATGTA
GATATTTGGCTTAAATATAGTTCCTAAGAAGCTTCTAATAAATTATACGA
ATTAAAAAAGATGGTTTTTTTCCTGATTA

Target sequence spanning *Nkx2-1* transgene to polyA tail used to design the *Nkx2-1* exogenous-only probe:
GCTTTATGGTCGGACCTGGTGAGTCGACCCGGGCGGCCGCTTCGAGCAGA
CATGATAAGATACATTGATGAGTTTGGACAAACCACAACTAGAATGCAGT
GAAAAAAATGCTTTATTTGTGAAATTTGTGATGCTATTGCTTTATT

Intracellular Flow Cytometry
Samples were monodispersed by trypsinization and fixed in 1.6% PFA in PBS for 30 min at 37ºC. Samples were stored for up to two weeks in PBS with 0.5% BSA and 0.02% Sodium Azide (NaN_3) at 4ºC before staining. To stain, samples were rinsed twice in 1X Saponin buffer (Permeability Wash Buffer 10x, Biolegend 421002). Primary antibodies were added in 1X Saponin buffer at the dilutions stated below and incubated for one hour at room temperature. Samples were rinsed twice with 1X Saponin buffer and then incubated with the secondary antibodies in 1X Saponin for 30 min at room temp. They were then rinsed twice with 1X Saponin and transferred to PBS with 2% FBS into filter-top FACS tubes (Falcon, 352235). Flow cytometry data was acquired from the BD FACSCalibur using the BD CellQuest software. Exported sample data was gated and analyzed as shown in the figures and text using the

FlowJo v10 software. Flow cytometry controls included unstained cells, cells incubated with the secondary antibody only (no primary), isotype controls, and negative controls (undifferentiated cells or cell populations known not to express the protein of interest).

Live Cell Surface Marker Staining

Cultures were monodispersed with trypsin and rinsed with FACS buffer containing HBSS with 2% FBS. Cells were incubated with conjugated primary antibody for 30 min at 4ºC. Cells were rinsed twice with FACS buffer and then transferred to filter-top polystyrene FACS tubes to run on the BD FACSCalibur. Flow cytometry controls included unstained cells and cells incubated with an isotype.

Live Cell Sorting

Cells were prepared as described in Surface Marker Staining. 10 µM Calcein Blue, AM (Life Technologies, C1429) was added to stain cells for inclusive live gating. Sorting was performed in the Boston University Flow Cytometry Core Facility using the FACSARIA II SORP high speed cell sorter. Cells sorted at day 6 were replated onto gelatin-coated plates with 24 hours exposure to ROCK inhibitor.

Purification of Nkx2-1^{GFP+} Thyroid and Forebrain mouse embryonic cells

All mouse work was approved by the Institutional Animal Care and Use Committee of Boston University School of Medicine. Thyroid epithelial cells and forebrain cells were isolated from mouse embryos using the Nkx2-1^{GFP} reporter mouse, originally described in (Longmire et al., 2012). Briefly, breeding cages were set up with one male and three female mice and the morning of the day a vaginal plug was detected was defined as embryonic day E0.5. Thyroid epithelial cells were sorted from E13.5 embryos and forebrain cells from E9.0 and E13.5 embryos. Timed-pregnant females were euthanized by inhalation of isoflurane and subsequent cervical dislocation. Embryos were delivered by cesarean and the three Nkx2-1^{GFP}-expressing domains (forebrain, thyroid, and lung) were dissected out with the help of an Olympus stereo fluorescence imaging microscope (model SZX16, Olympus America, Central Valley, PA) and kept in HBSS with 10% FBS. Tissues were digested using Collagenase A (0.1%, Roche 103578) and Dispase II (2.4 U/ml, Roche 295825) for 60 min at 37ºC with periodic trituration. Monodispersed cells were resuspended in HBSS with 2% FBS, filtered through 30 µm FACS strainers and stained with PI (for dead cell exclusion) directly before sorting. Sorting was performed in the Boston University Flow Cytometry Core Facility using the FACSARIA II SORP high speed cell sorter.

Measurement of T4 by ELISA

T4 levels in mature organoids were measured as previously described (Kurmann et al., 2015). Organoids were removed from the Matrigel using Dispase and were lysed with 330 µl per sample of cold Barbital buffer (Sigma, B5934) using the QIAGEN TissueLyser system. Lysate from the organoids was sonicated and centrifuged for 20 min at 13,000 rpm. The supernatant was divided into three groups for genomic DNA (gDNA) extraction, and enzyme degraded and non-degraded samples.

For enzymatic degradation to break down T4 from TG-T4, 150 µl of protease solution (Kurmann et al., 2015) and 15 µl of Toluene (Sigma, 244511) were added to 100 µl of lysate and incubated for 48 hours at 37°C with shaking followed by 5 min at 98°C for enzyme inactivation. T4 concentration was measured using AccuDiag T4 ELISA kit (Diagnostic automation/Cortez Diagnostics, Inc., 3149-18). 25 µl of degraded or non-degraded organoid lysates were used for measurement and normalized to gDNA concentration.

Genomic DNA was extracted using Archive Pure DNA tissue kit (5Prime, 2300860). Briefly, 300 µl of Cell Lysis Solution was added to 100 µl of organoid lysate followed by treatment with RNase A Solution. After incubation for 5 min at 37°C, 100 µl of Protein Precipitation Solution was added to the lysate. After centrifugation, the supernatant containing the gDNA was mixed with 300 µl of isopropanol and centrifuged for one hour at 4°C. The gDNA pellet was washed with 70% ethanol and hydrated with 15 µl of DNA Hydration Solution. The concentration of gDNA was measured using the Nanodrop spectrophotometer.

SPC-dsRed Lentivirus Reporter

The SPC-dsRed lentivirus was generated as previously described (Longmire et al., 2012). In brief, a published 3.7 kb SPC promoter fragment was cloned upstream of the dsRed construct and packaged into the virus. Cells were transduced with the lentivirus on day 9 while in specification media. 8 µl of the virus per 1 ml media in a 6 well plate, with 5 µg/ml Polybrene (Sigma, H9268-50g) was incubated with the cells for 24 hrs. Dose was determined by parallel transduction with a CMV-dsRed surrogate reporter to estimate transduction efficiency. Cells were subsequently monitored for dsRed expression using fluorescence microscopy. At day 14, cells were passaged into FGF2+10 media

until day 22, then changed to DCI+K media to further stimulate maturation, as previously described (Longmire et al., 2012).

RNA Sequencing Preparation and Analysis

RNA samples were prepared for RNA-Sequencing as described in the Supplemental Experimental Procedures for RT-qPCR. Samples were selected from biologically replicate runs (separate differentiations), in duplicate or triplicate sets. D1 RNA was limited to duplicate samples due to available space on the Flow-Cell. Sequencing libraries were prepared from total RNA samples using Illumina® TruSeq® RNA Sample Preparation Kit v2. Briefly, the mRNA was isolated using magnetic bead-based poly(A) selection, fragmented, and randomly primed for reverse transcription, followed by second-strand synthesis to create double-stranded cDNA fragments. These cDNA fragments were then end-repaired, added with a single 'A' base, and ligated to Illumina® Paired-End sequencing adapters. The products were purified and PCR-amplified to create the final cDNA library. The libraries from individual samples were pooled in groups of four for cluster generation on the Illumina® cBot using Illumina® TruSeq® Paired-End Cluster Kit. Each sample was sequenced four per lane on the Illumina® HiSeq 2500 to generate more than 25 million Paired-End 100-bp reads. The RNA-Seq reads were aligned to mouse genome mm9 by Tophat v2.0.4 (Kim et al., 2013). Then the reads were summed to the gene level by HTSeq package (Anders et al., 2015). This data has been deposited in NCBI's Gene Expression Omnibus and are accessible through GEO Series accession number http://www.ncbi.nlm.nih.gov/geo/query/acc.cgi?acc=GSE92572.

A generalized linear model implemented by edgeR package was used to extract the differentially expressed genes between each two-condition comparison (D14 vs. D0, D7 vs. D0, D14 vs. D7) with a false discovery rate (FDR) cutoff at 0.05 (Robinson et al., 2010). Finally, a hierarchical clustering was performed on the combined differentially expressed gene list across all samples. Data were log-transformed with gene expression counts, mean centered, and row scaled. To generate the heat map, hierarchical agglomerative clustering was performed via Pearson correlation similarity metric with average linkage used to determine pairwise distance. Java Treeview (Saldanha, 2004) was used to generate the heat map visualization and for extraction of the gene lists comprising the main clusters.

Identification of Putative Cell Surface Markers and Transcriptional Regulators

Cell surface markers (cut-off of $p<0.001$) were identified using DAVID (Huang et al., 2009) through categorization in GO term "Integral to Plasma Membrane" (GO:0005887) and manually curated to exclude genes encoding for proteins not transmembrane or plasma membrane bound. Transcription factors (cut-off of $p<0.001$) were selected using correlation (4/5 or 5/5) with the five reference lists: Animal Transcription Factor DataBase (AnimalTFDB v2.0 2014-06-30) (Zhang et al., 2012), Riken Transcription Factor Database, TFdb (Kanamori et al., 2004), TFcheckpoint (Transcription Factor Checkpoint, (Chawla et al., 2013)), and classification by DAVID within GO terms "Transcription Factor Activity" (GO:0003700) and "DNA Binding" (GO:0003677). Small-scale heat maps in the figures were generated using GENE-E (http://www.broadinstitute.org/cancer/software/GENE-E/).

Gene Ontology Analysis

Lists of significantly (FDR <0.05) differentially expressed genes were entered into the Gene Ontology Consortium online resource (Ashburner et al., 2000; Consortium, 2015). GO terms with a p-value of <0.05 were entered into the REVIGO website for consolidation (Supek et al., 2011), using PANTHER Overrepresentation Test (release 2015-04-30) and GO Ontology database (release 2015-08-06). The log10 p-values of the GO term output were used for the graphical representation of associated biological processes (Figure S4A).

GSEA analysis

Genes from the "Early" and "Late" clusters were ranked on logFC values. Gene sets were selected from 'gene set data for pathway analysis in mouse' R package (Bares V and Ge X (2015). gskb: Gene Set data for pathway analysis in mouse. R package version 1.2.0). Specifically, we used all the provided 259 KEGG gene sets from the 'Metabolic pathways' set and all 12525 GO gene sets from the 'Gene Ontology'. The command-line version of GSEA (Mootha et al., 2003; Subramanian et al., 2005) was used in the 'Preranked' mode (specifically: gsea2-2.1.0.jar -Xmx512m xtools.gsea.GseaPreranked) and 'classic' scoring scheme, as advised for RNA-Seq data in the FAQ section of GSEA online documentation. We ran GSEA with the default parameters. Gene sets included in the figure were selected based on a cutoff of FDR < 0.2.

Principal Component Analysis

Before PCA, expression values were normalized across all samples to a mean of zero and a standard deviation of one. PCA of the normalized data was performed using the sklearn.decomposition.PCA command in the Python package scikit-learn.

Gene Expression Projections

Here we give a brief overview of the projection method plots shown in Figure 4F-H, please see (Lang et al., 2014; Pusuluri et al., 2015) for complete mathematical details. The projection method allows one to compare experimentally acquired gene expression data versus a reference basis. A projection score of 1.0 indicates a perfect match of gene expression, while 0.0 indicates no match. The projection method has several key advantages relative to other techniques such as PCA. First, it provides a biologically interpretable numeric value of the similarity between the data and the reference basis. Second, it removes the inherent correlations of the reference basis by measuring orthogonal projections onto the reference basis. This means that each reference cell type has a projection of 1 with only itself and has a projection of 0 with all other reference cell types.

To create the reference basis cell types, we first started with the basis used in (Lang et al., 2014; Pusuluri et al., 2015). We removed the following cell types: Common Lymphoid Progenitor (CLP), Common Myeloid Progenitor (CMP), Granulocyte-Monocyte Progenitor (GMP), and Megakaryocyte-Erythroid Progenitor (MEP). Second, we included E8.25 ectoderm, E8.25 foregut, and E14.5 Nkx2-1^{+} thyroid RNA-Seq samples from our lab. The basis thus consists of 62 cell types.

The dataset consists of a mix of Affymetrix GeneChip Mouse Gene 1.0 ST and RNA-Seq data and was normalized as follows. First, raw microarrays and RNA-Seq were separately processed following standard techniques for each data type. Next, only genes common to all datasets were kept, leading to N=12039 genes. In order to make robust comparisons across platforms the raw expression output was converted to a rank order. Next, we wanted to convert this rank order to the z-score of a log-normal distribution. We converted the rank to a percentile (for N genes, by dividing by N+1), and then this percentile into a normal z-score. For mathematical convenience, we used a biased estimator (i.e. we normalized by N and not N-1) since then the Euclidean norm of each microarray gene expression was N. Therefore, for the data analysis each sample is described by a Gaussian distribution with a Euclidean norm of N = 12039.

As mentioned above, a projection score of 1.0 indicates a perfect match of gene expression, 0 indicates no match, and -1.0 indicates perfectly anti-correlated gene expression. There are no direct equivalents of p-values to measure the significance of a projection. However, one can compare the expression of random sets of gene expression versus the reference basis. A random set of 10,000 different gene expression profiles (each with N=12039 genes) had a mean projection of 0 (within machine precision) with any of the reference cell types, while the standard deviation of the projections was 0.0184. Therefore, a projection greater in magnitude of 0.092 (5 stds) is highly unlikely to be due to random expression patterns. This is also supported by the fact that the variation in the projections of each experimental replicate was minimal.

Simple mathematical model for bistable switch

The experimental data in the main text is consistent with the idea that Nkx2-1 positively regulates its own expression, giving rise to a bistable switch. To demonstrate this, we constructed a simple model of a genetic switch consisting of a gene which produces a protein that can bind its own promoter and increase gene expression (Figure 4F). When the feedback loop is cooperative, this molecular architecture can give rise to bistability, with two stable steady-states possible: (i) a low-expression steady-state where the positive feedback loop is off and proteins are expressed at low levels and (ii) a high-expression steady-state where the positive feedback loop is turned-on and proteins are expressed at high levels (Ferrell, 2002; Maamar et al., 2007; Mehta et al., 2008; Tyson et al., 2003).

Mathematically, we represent the deterministic dynamics of such a bistable switch using a simple differential equation for the number of mRNA molecules, *m*, and the number of protein molecules, *p*:

$$\frac{dm}{dt} = \alpha_{pulse}(t) + \alpha_0 + \frac{a_m p^q}{p^q + K_d^q} - \tau_m^{-1} m \quad (1)$$

$$\frac{dp}{dt} = a_p m - \tau_p^{-1} p \quad (2)$$

with $\alpha_{\mathrm{pulse}}(\mathrm{t})$ the generally (time-dependent) transcription rate from the pulsing construct, α_0 the basal transcription rate, a_m the maximal transcription rate due to the positive feedback loop, K_d the half-maximal protein concentration for the positive feedback loop to turn on, q the Hill coefficient describing cooperative binding, τ^m the mRNA lifetime, a_p the rate at which proteins are translated from an mRNA molecule, and τ^p the protein lifetime. For all simulations, we take (where rates are in units of molecules per hour) $\alpha_0 = 0.5$, $a_m = 5$, $a_p = 20$. Additionally, $\tau^p = 6$hr, $\tau^m = 0.5$hr, q = 3, and $K_d = 150$. Furthermore, we assume there is a finite time window during which the cell can switch to high to a protein state. Very little is known about how this

occurs at the molecular level. Inspired by measurements of the transition to competence in the bacteria Bacillus subtilis (Maamar and Dubnau, 2005; Maamar et al., 2007), we model this process by assuming that the basal transcription rate is turned off after a critical time cutoff, t = 25hr so that $\alpha_0 = 0.5\theta(t_{cutoff} - t)$, where $\theta(t)$ is the Heaviside function. We emphasize that this is just one of many ways that this regulation could occur and our results do not depend strongly on this choice. To model pulsing for a duration t_{pulse}, we use $a_{pulse} = 4 * \theta(t - t_{pulse})$.

One can easily verify that with this choice of parameters, the dynamics are bistable with critical concentration $p_{crit} \approx 102$ separating the low-expression and high-expression fixed points. When $p < p_{crit}$, the cell is attracted to a low-expression fixed point. However, when $p > p_{crit}$, cell are attracted to a high expression state. Due to stochastic effects resulting from low number of molecules, cells can transition between these steady-states.

To understand the stochastic switching dynamics, we performed a stochastic simulation of gene expression dynamics for this system using Gillespie's algorithm (Gillespie, 1977; Mehta et al., 2008). We considered three distinct conditions: (i) no pulse where $t_{pulse} = 0$, (ii) short pulses where $t_{pulse} = 2hr$, and (iii) a long pulse where $t_{pulse} = 24hr$. For each of these conditions, we performed 1000 simulations and calculated the fraction of cells with high protein expression ($p > p_{crit}$) at $t = 100hr$ (Figure 4G). As expected, the fraction of high-expression cells increased with the pulse duration. We also examined the time traces for cells that switched or did not switch in both the pulsed and non-pulsed conditions, representative traces are shown (Figure 4H).

As shown in Figure 4F, although a certain percentage of cells is expected to reach the "On" state without an exogenous NKX2-1 pulse, this percentage could be increased by short or long NKX2-1 pulses. Figure 4H simulations exemplify this effect, as cells displayed heterogeneous behaviors with some cells reaching the "On" expression state (purple lines) and others reaching the "Off" expression state in all conditions. On the other hand, the "On" expression state is favored in the pulsed condition and it is achieved faster than in the non-pulsed condition.

Supplemental References

Anders, S., Pyl, P.T., and Huber, W. (2015). HTSeq--a Python framework to work with high-throughput sequencing data. Bioinformatics *31*, 166-169.

Ashburner, M., Ball, C.A., Blake, J.A., Botstein, D., Butler, H., Cherry, J.M., Davis, A.P., Dolinski, K., Dwight, S.S., Eppig, J.T., *et al.* (2000). Gene ontology: tool for the unification of biology. The Gene Ontology Consortium. Nat Genet *25*, 25-29.

Chawla, K., Tripathi, S., Thommesen, L., Laegreid, A., and Kuiper, M. (2013). TFcheckpoint: a curated compendium of specific DNA-binding RNA polymerase II transcription factors. Bioinformatics *29*, 2519-2520.

Consortium, G.O. (2015). Gene Ontology Consortium: going forward. Nucleic Acids Res *43*, D1049-1056.

Ferrell, J.E. (2002). Self-perpetuating states in signal transduction: positive feedback, double-negative feedback and bistability. Curr Opin Cell Biol *14*, 140-148.

Gadue, P., Huber, T.L., Paddison, P.J., and Keller, G.M. (2006). Wnt and TGF-beta signaling are required for the induction of an in vitro model of primitive streak formation using embryonic stem cells. Proc Natl Acad Sci U S A *103*, 16806-16811.

Gillespie, D.T. (1977). EXACT STOCHASTIC SIMULATION OF COUPLED CHEMICAL-REACTIONS. J Phys Chem *81*, 2340-2361.

Gouon-Evans, V., Boussemart, L., Gadue, P., Nierhoff, D., Koehler, C.I., Kubo, A., Shafritz, D.A., and Keller, G. (2006). BMP-4 is required for hepatic specification of mouse embryonic stem cell-derived definitive endoderm. Nat Biotechnol *24*, 1402-1411.

Huang, D.W., Sherman, B.T., and Lempicki, R.A. (2009). Systematic and integrative analysis of large gene lists using DAVID bioinformatics resources. Nat Protoc *4*, 44-57.

Kanamori, M., Konno, H., Osato, N., Kawai, J., Hayashizaki, Y., and Suzuki, H. (2004). A genome-wide and nonredundant mouse transcription factor database. Biochem Biophys Res Commun *322*, 787-793.

Kim, D., Pertea, G., Trapnell, C., Pimentel, H., Kelley, R., and Salzberg, S.L. (2013). TopHat2: accurate alignment of transcriptomes in the presence of insertions, deletions and gene fusions. Genome biology *14*, R36.

Kurmann, A.A., Serra, M., Hawkins, F., Rankin, S.A., Mori, M., Astapova, I., Ullas, S., Lin, S., Bilodeau, M., Rossant, J., *et al.* (2015). Regeneration of Thyroid Function by Transplantation of Differentiated Pluripotent Stem Cells. Cell Stem Cell *17*, 527-542.

Lang, A.H., Li, H., Collins, J.J., and Mehta, P. (2014). Epigenetic Landscapes Explain Partially Reprogrammed Cells and Identify Key Reprogramming Genes. PLoS Comput Biol *10*.

Livak, K.J., and Schmittgen, T.D. (2001). Analysis of relative gene expression data using real-time quantitative PCR and the 2(-Delta Delta C(T)) Method. Methods *25*, 402-408.

Longmire, T.A., Ikonomou, L., Hawkins, F., Christodoulou, C., Cao, Y.X., Jean, J.C., Kwok, L.W., Mou, H.M., Rajagopal, J., Shen, S.S., *et al.* (2012). Efficient Derivation of Purified Lung and Thyroid Progenitors from Embryonic Stem Cells. Cell Stem Cell *10*, 398-411.
Maamar, H., and Dubnau, D. (2005). Bistability in the Bacillus subtilis K-state (competence) system requires a positive feedback loop. Mol Microbiol *56*, 615-624.
Maamar, H., Raj, A., and Dubnau, D. (2007). Noise in gene expression determines cell fate in Bacillus subtilis. Science *317*, 526-529.
Mehta, P., Mukhopadhyay, R., and Wingreen, N.S. (2008). Exponential sensitivity of noise-driven switching in genetic networks. Phys Biol *5*, 6.
Mootha, V.K., Lindgren, C.M., Eriksson, K.F., Subramanian, A., Sihag, S., Lehar, J., Puigserver, P., Carlsson, E., Ridderstrale, M., Laurila, E., *et al.* (2003). PGC-1 alpha-responsive genes involved in oxidative phosphorylation are coordinately downregulated in human diabetes. Nature Genet *34*, 267-273.
Pusuluri, S.T., Lang, A.H., Mehta, P., and Castillo, H.E. (2015). Cellular reprogramming dynamics follow a simple one-dimensional reaction coordinate. arXiv *1505.03889 [q-bio.MN]*
Robinson, M.D., McCarthy, D.J., and Smyth, G.K. (2010). edgeR: a Bioconductor package for differential expression analysis of digital gene expression data. Bioinformatics *26*, 139-140.
Saldanha, A.J. (2004). Java Treeview-extensible visualization of microarray data. Bioinformatics *20*, 3246-3248.
Schindelin, J., Arganda-Carreras, I., Frise, E., Kaynig, V., Longair, M., Pietzsch, T., Preibisch, S., Rueden, C., Saalfeld, S., Schmid, B., *et al.* (2012). Fiji: an open-source platform for biological-image analysis. Nat Methods *9*, 676-682.
Schneider, C.A., Rasband, W.S., and Eliceiri, K.W. (2012). NIH Image to ImageJ: 25 years of image analysis. Nat Methods *9*, 671-675.
Subramanian, A., Tamayo, P., Mootha, V.K., Mukherjee, S., Ebert, B.L., Gillette, M.A., Paulovich, A., Pomeroy, S.L., Golub, T.R., Lander, E.S., *et al.* (2005). Gene set enrichment analysis: A knowledge-based approach for interpreting genome-wide expression profiles. Proc Natl Acad Sci U S A *102*, 15545-15550.
Supek, F., Bošnjak, M., Škunca, N., and Šmuc, T. (2011). REVIGO summarizes and visualizes long lists of gene ontology terms. PloS One *6*, e21800.
Tyson, J.J., Chen, K.C., and Novak, B. (2003). Sniffers, buzzers, toggles and blinkers: dynamics of regulatory and signaling pathways in the cell. Curr Opin Cell Biol *15*, 221-231.
Zhang, H.M., Chen, H., Liu, W., Liu, H., Gong, J., Wang, H.L., and Guo, A.Y. (2012). AnimalTFDB: a comprehensive animal transcription factor database. Nucleic Acids Res *40*, D144-D149.